# WILLMAN 1—A PROBABLE DWARF GALAXY WITH AN IRREGULAR KINEMATIC DISTRIBUTION

BETH WILLMAN[1], MARLA GEHA[2], JAY STRADER[3,7], LOUIS E. STRIGARI[4],
JOSHUA D. SIMON[5], EVAN KIRBY[6,8], NHUNG HO[2], AND ALEX WARRES[1]

[1] Departments of Physics and Astronomy, Haverford College, Haverford, PA 19041, USA; bwillman@haverford.edu, awarres@haverford.edu
[2] Astronomy Department, Yale University, New Haven, CT 06520, USA; marla.geha@yale.edu
[3] Harvard-Smithsonian CfA, Cambridge, MA 02144, USA; jstrader@cfa.harvard.edu
[4] Kavli Institute for Particle Astrophysics and Cosmology, Stanford University, Stanford, CA 94305, USA; strigari@stanford.edu
[5] Observatories of the Carnegie Institution of Washington, Pasadena, CA 91101, USA; jsimon@obs.carnegiescience.edu
[6] California Institute of Technology, Pasadena, CA 91106, USA; enk@astro.caltech.edu

## ABSTRACT

We investigate the kinematic properties and stellar population of the Galactic satellite Willman 1 (Wil 1) by combining Keck/DEIMOS spectroscopy with Kitt Peak National Observatory mosaic camera imaging. Wil 1, also known as SDSS J1049+5103, is a nearby, ultra-low luminosity Milky Way companion. This object lies in a region of size–luminosity space ($M_V \sim -2$ mag, $d \sim 38$ kpc, $r_{\rm half} \sim 20$ pc) also occupied by the Galactic satellites Boötes II and Segue 1 and 2, but no other known old stellar system. We use kinematic and color–magnitude criteria to identify 45 stars as possible members of Wil 1. With a systemic velocity of $v_{\rm helio} = -12.8 \pm 1.0$ km s$^{-1}$, Wil 1 stars have velocities similar to those of foreground Milky Way stars. Informed by Monte Carlo simulations, we identify 5 of the 45 candidate member stars as likely foreground contaminants, with a small number possibly remaining at faint apparent magnitudes. These contaminants could have mimicked a large velocity dispersion and abundance spread in previous work. The significant spread in the [Fe/H] of the highly likely Wil 1 red giant branch members ([Fe/H] = $-1.73 \pm 0.12$ and $-2.65 \pm 0.12$) supports the scenario that Wil 1 is an ultra-low luminosity dwarf galaxy, or the remnants thereof, rather than a star cluster. However, Wil 1's innermost stars move with radial velocities offset by 8 km s$^{-1}$ from its outer stars and have a velocity dispersion consistent with 0 km s$^{-1}$, suggesting that Wil 1 may not be in dynamical equilibrium. The combination of the foreground contamination and unusual kinematic distribution make it difficult to robustly determine the dark matter mass of Wil 1. As a result, X-ray or gamma-ray observations of Wil 1 that attempt to constrain models of particle dark matter using an equilibrium mass model are strongly affected by the systematics in the observations presented here. We conclude that, despite the unusual features in the Wil 1 kinematic distribution, evidence indicates that this object is, or at least once was, a dwarf galaxy.

*Key words:* galaxies: dwarf – galaxies: individual (Willman 1) – galaxies: kinematics and dynamics – galaxies: star clusters: general

*Online-only material:* color figures

## 1. INTRODUCTION

Since 2004, over a dozen Milky Way satellites have been discovered via slight statistical overdensities of individual stars in the Sloan Digital Sky Survey (SDSS) catalog and confirmed by both follow-up imaging and spectroscopy (e.g., Willman et al. 2005a, 2005b; Zucker et al. 2006a, 2006b; Belokurov et al. 2006, 2007, 2008, 2009; Sakamoto & Hasegawa 2006; Irwin et al. 2007; Walsh et al. 2007). These satellites are dominated by old stellar populations and have absolute magnitudes of $-8$ mag $< M_V < -1$ mag. Their median $M_V$ is $\sim -4$, less luminous than the median observed for Milky Way globular clusters (GCs; Harris 1996). Stellar kinematics consistent with mass-to-light (M/L) ratios >100 demonstrate that most of these objects are dark matter dominated dwarf galaxies (Muñoz et al. 2006; Simon & Geha 2007; Martin et al. 2007; Strigari et al. 2008a).

Four of the new Milky Way companions—Willman 1 (Wil 1), Boötes II, Segue 1, and Segue 2—contain $L \lesssim 1000 L_\odot$ and have been difficult to classify. With estimated $r_{\rm half}$ of 20–40 pc, these four objects lie in a gap between the sizes of known old stellar populations (Milky Way GCs and dwarf

spheroidals) in size–luminosity space. They are less luminous than all but three known objects classified as GCs, providing few stars bright enough for kinematic study (Willman et al. 2005a; Belokurov et al. 2007, 2009; Walsh et al. 2008). Moreover, their proximity to the Milky Way ($d \lesssim 40$ kpc) and their possible embedding in the Sagittarius stream (Boötes II and Segue 1 and 2; Belokurov et al. 2009; Niederste-Ostholt et al. 2009—although see Law & Majewski 2010) complicate the interpretation of their observed properties.

Measuring the dark mass content of satellites with $M_V > -3$ is a critical ingredient to our understanding of the size and mass scale of dark matter clustering, the abundance and distribution of dark matter halos, and the extreme low mass limit of galaxy formation. Koposov et al. (2007) and Walsh et al. (2009) showed that Milky Way companions fainter than $M_V \sim -3$ could not have been discovered at all in SDSS if they are more distant than $\sim 50$ kpc from the Sun. They may thus represent the tip of an iceberg of such objects around the Milky Way (e.g., Tollerud et al. 2008). Moreover, these objects have been shown to be excellent targets for observations seeking the gamma-ray signature of annihilating dark matter (Strigari et al. 2008b; Geha et al. 2009).

Two primary lines of reasoning have been used to argue for dark matter content in, and thus a galaxy classification for, these

---

[7] Hubble Fellow, now Menzel Fellow.

[8] Hubble Fellow.

four extreme objects: (1) a kinematic distribution that is unbound without dark matter (Segue 1 and 2: Geha et al. 2009; Belokurov et al. 2008) and/or (2) a spectroscopically observed spread in [Fe/H], which is not expected in purely stellar systems with a total mass as low as the observable baryonic masses of the ultra-faint dwarfs (Wil 1: Martin et al. 2007). Thus far, the strongest evidence for a substantial dark mass component has been provided by the line-of-sight velocities of stars in the Segue 1 object. Geha et al. (2009) analyzed 24 member stars observed with DEIMOS to find $(M/L_V)_{central} > 1000$. Simon et al. (2011) confirm this result with a larger sample of 71 member stars. Circumstantial lines of reasoning have also been used to argue that Boötes II may contain a substantial dark matter component (Walsh et al. 2008).

The reliability of these kinematic or spectroscopic [Fe/H] analyses of nearby dwarf galaxies hinge on having samples of member stars that are as contamination free as possible, and a quantitative calculation of the unavoidable contamination that may be present. Contaminants may be stars from the Milky Way, from unrelated stellar streams such as Sagittarius, or from an unbound component of the dwarf galaxy itself. With a set of only ∼10–50 member star velocities, a small number of interlopers could artificially inflate the observed velocity dispersion, leading to an overestimate of the mass-to-light ratio. With only a few stars in each of these systems bright enough for a spectroscopic [Fe/H] measurement, just one or two interloper stars at bright apparent magnitudes could mimic an [Fe/H] spread. Foreground Milky Way thick disk and halo stars (at the photometric depths reachable by spectroscopy) contaminate the color–magnitude diagrams (CMDs) of these extreme satellites. Segue 1 and Boötes II have systemic velocities of $-206 \pm 1.3$ km s$^{-1}$ (Geha et al. 2009) and $-117$ km s$^{-1}$ (Koch et al. 2009), respectively, which are offset from the majority of thick disk and halo stars. However, both Wil 1 ($v_{sys} = -13.3 \pm 2.5$ km s$^{-1}$; Martin et al. 2007) and Segue 2 ($v_{sys} = -40$ km s$^{-1}$; Belokurov et al. 2009) have systemic velocities that substantially overlap with the velocities of Milky Way stars, making the identification of interlopers particularly difficult.

Wil 1 (SDSS J1049+5103), located at $(\alpha_{2000}, \delta_{2000}) = (162°343, 51°051)$, is an old, metal-poor Milky Way satellite at a distance of $38 \pm 7$ kpc with $M_V \sim -2$ mag (Willman et al. 2005a; Martin et al. 2008a). Based on equilibrium models of its mass, this object has been claimed to have a high dark matter content (Geha et al. 2009; Wolf et al. 2010). A high dark matter content plus its relative proximity would make it a promising source of gamma rays from annihilating dark matter (Strigari et al. 2008b). As a result of this prediction, several groups have attempted to investigate the particle nature of dark matter via gamma-ray (Essig et al. 2009; Aliu et al. 2009) and X-ray (Loewenstein & Kusenko 2010) observations. However, its possibly irregular spatial distribution supports the idea that it is tidally disturbed (Willman et al. 2006; Martin et al. 2007) which could mean that its kinematics do not faithfully trace its gravitational potential. Although Martin et al. (2007) argued that Wil 1's classification of a dwarf galaxy was supported by an observed spread in the [Fe/H] of its member stars, such spectroscopic studies of Wil 1 suffer particularly from the presence of interloper stars. Its systemic velocity is similar to the velocities of Milky Way foreground stars with colors and magnitudes consistent with Wil 1 membership. Siegel et al. (2008) showed that contamination from Milky Way stars was a problem in the Martin et al. (2007) study and found that 2–5 of the 7 Wil 1 spectroscopic red giant branch (RGB) "members" were

actually Milky Way foreground stars. These foreground stars might have generated the apparent spread in [Fe/H].

To address the present uncertainties in the nature of the Wil 1 object, we present DEIMOS observations of 45 probable member stars. We carefully characterize the possible contamination in this sample, and then use it to study the abundances and kinematics of stars in Wil 1. In Section 2, we discuss target selection and data reduction for our DEIMOS slit masks. Selecting Wil 1 member stars, including a detailed discussion of foreground contamination, is presented in Section 3. In Section 4, we discuss whether Wil 1 appears to be a star cluster or a dwarf galaxy, and then analyze Wil 1's kinematics in Section 5.

## 2. DATA

### 2.1. Photometry

The data are from wide-field imaging of Wil 1 with the mosaic imager on the 4 m telescope at Kitt Peak National Observatory (KPNO) on 2005 April 7 and 8. The reduction, photometry, and calibration of these data used in this paper are identical to those presented in Willman et al. (2006). We briefly describe here the reduction, photometry, and photometric calibration of these data. See Willman et al. (2006) for more details.

Ten 600 s exposures were taken through each of the SDSS $g$ and $r$ filters, with seeing varying between 1″2 and 1″4. Photometry was performed on each individual exposure and then averaged to yield a stellar catalog with excellent photometry and star–galaxy separation at the apparent magnitudes we are investigating.

Stellar magnitudes were photometrically calibrated with the SDSS Data Release 4 (Adelman-McCarthy et al. 2006) stellar catalog. The apparent magnitudes were then corrected for extinction using the Schlegel et al. (1998) dust map values given in the SDSS catalog. The average $E(g - r)$ along the line of sight to Wil 1 is 0.014. All magnitudes in this paper are de-reddened; we use the subscript "$_0$" to denote that the colors and magnitudes are de-reddened. At magnitudes brighter than $r_0 = 17.0$, we replaced the KPNO photometry with the point-spread function (PSF) photometry from SDSS Data Release 7 (Abazajian & Sloan Digital Sky Survey 2009).

Figure 1 shows the CMD of all point sources within two elliptical half-light radii of the center of Wil 1, using the structural parameters derived by Martin et al. (2008b). The points in this CMD delineate the main sequence (MS) of Wil 1, with candidate RGB stars visible. Dotted boxes outline the liberal color–magnitude (CM) selection that we will use in the rest of this paper as the CM requirements for possible Wil 1 membership.

We applied the CM selection shown in Figure 1 to this photometric catalog to calculate a revised center of Wil 1. We began with the center, based on the much shallower SDSS data set, calculated by Martin et al. (2008b), and then iteratively calculated the average position of stars within 2 arcmin of the center until we converged on $(\alpha_{2000}, \delta_{2000}) = (162.3397, 51.0508)$. We will use this center for the rest of the paper.

### 2.2. Spectroscopic Target Selection

Stars in Wil 1 were targeted for spectroscopy using the photometric catalog described in the previous section. We set the target priorities to preferentially observe stars with a high likelihood of being Wil 1 members based on their color, magnitude, and spatial position. First priority was given to stars
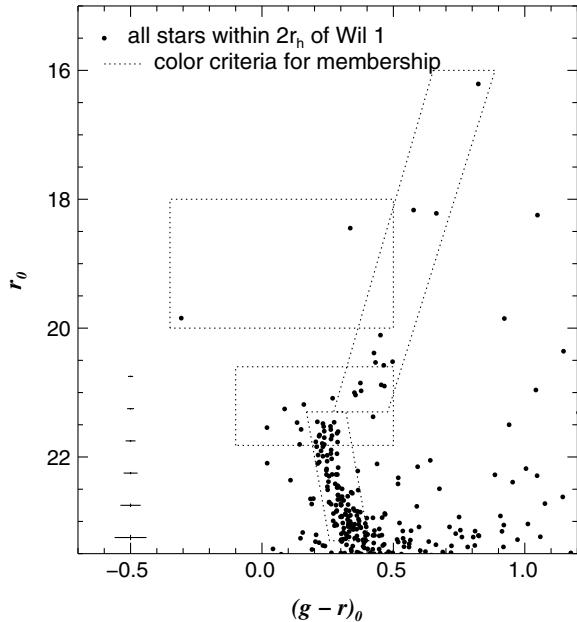
**Figure 1.** De-reddened color–magnitude diagram of all stars within two elliptical half-light radii of the center of Willman 1 from KPNO $g$- and $r$-band photometry. We used (position angle, ellipticity, $r_{half}$) = (77,0.47, 2′.3) from Martin et al. (2008a) to calculate half-light distances. The region inside the dotted boxes is the location of our highest priority spectroscopic selection criteria, hereafter referred to as the color criteria used to identify stars possibly belonging to Wil 1. The sizes of color and magnitude uncertainties are shown by the crosses on the left of the CMD.

that (1) spatially overlap the main body of Wil 1 and (2) reside within regions of the CMD that are consistent with the MS and turnoff, horizontal branch, and RGB of an old stellar population at the distance of Wil 1. These CM criteria are shown by the dotted lines overplotted in Figure 1. We chose to implement liberal, rectangular CM criteria to include Wil 1 member stars with a range of possible [Fe/H] and ages in our spectroscopic sample. Second priority was given to stars occupying a similar CM region, independent of spatial location. All remaining stars were assigned third priority. Within each of these three tiers, stars were further prioritized by their apparent magnitude, with the brightest stars receiving highest priority. An average of 100 slitlets were placed on each mask (see Table 1).

### 2.3. Spectroscopy and Data Reduction

Four multislit masks were observed for Wil 1 using the Keck II 10 m telescope and the DEIMOS spectrograph (Faber et al. 2003). Three masks were observed on the nights of 2006 November 20–22, the fourth was observed on 2007 March 20. Exposure times, mask positions, and additional observing details are given in Table 1. The masks were observed with the 1200 line mm$^{-1}$ grating covering a wavelength region 6400–9100 Å. The spatial scale is 0′′.12 pixel$^{-1}$, the spectral dispersion of this setup is 0.33 Å, and the resulting spectral resolution is 1.37 Å (FWHM). Slitlets were 0′′.7 wide. The seeing conditions during both runs were on average ~0′′.75. Despite the similar observing conditions, few spectra were usable from the fourth mask because the targeted stars were fainter. The minimum slit length was 4′′ to allow adequate sky subtraction; the minimum spatial separation between slit ends was 0′′.4 (3 pixels).

Spectra were reduced using a modified version of the spec2d software pipeline (version 1.1.4) developed by the DEEP2

**Table 1**
Keck/DEIMOS Multi-slit mask Observations of Willman 1

| Mask Name | $\alpha$ (J2000) (h:m:s) | $\delta$ (J2000) (°:′:″) | P.A. (deg) | $t_{exp}$ (s) | No. of Slits | % Useful Spectra |
|---|---|---|---|---|---|---|
| Wil1_1 | 10:49:23 | +51:01:20 | 75 | 5 × 1800 | 110 | 58% |
| Wil1_2 | 10:49:40 | +51:01:57 | 110 | 5 × 1800 | 94 | 45% |
| Wil1_3 | 10:49:11 | +51:02:16 | 20 | 3 × 1800 | 92 | 50% |
| Wil1_4 | 10:49:24 | +51:01:02 | −5 | 3 × 1800 | 127 | 7% |

**Notes.** Right ascension, declination, position angle, and total exposure time for each Keck/DEIMOS slit mask in Willman 1. The final two columns refer to the total number of slitlets on each mask and the percentage of those slitlets for which a redshift was measured. Mask 4 has a low efficiency because many faint stars were targeted.

team at the University of California-Berkeley for that survey. A detailed description of the two-dimensional reductions can be found in Simon & Geha (2007). The final one-dimensional spectra are rebinned into logarithmically spaced wavelength bins with 15 km s$^{-1}$ pixel$^{-1}$.

### 2.4. Radial Velocities and Error Estimates

We measure radial velocities and estimate velocity errors using the method detailed in Simon & Geha (2007). We refer the reader to this paper for a description of the method and only highlight the important steps below.

Radial velocities were measured by cross-correlating the observed science spectra with a series of high signal-to-noise (S/N) stellar templates. The templates were observed with Keck/DEIMOS using the same setup as described in Section 2.3 and cover a wide range of stellar types (F8 to M8 giants, subgiants, and dwarf stars) and metallicities ([Fe/H] = −2.12 to +0.11). We calculate and apply a telluric correction to each science spectrum by cross-correlating a hot stellar template with the night sky absorption lines following the method in Sohn et al. (2007). The telluric correction accounts for the velocity error due to miscentering the star within the 0′′.7 slit caused by small mask rotations or astrometric errors. We apply both a telluric and heliocentric correction to all velocities presented in this paper.

It is crucial to accurately assess our velocity errors because the internal velocity dispersion of Wil 1 is expected to be comparable to the DEIMOS velocity errors associated with individual measurements. We determine the random component of our velocity errors using a Monte Carlo bootstrap method. Noise is added to each pixel in the one-dimensional science spectrum. We then recalculate the velocity and telluric correction for 1000 noise realizations. Error bars are defined as the square root of the variance in the recovered mean velocity in the Monte Carlo simulations. The systematic contribution to the velocity error was determined by Simon & Geha (2007) to be 2.2 km s$^{-1}$ based on repeated independent measurements of individual stars, and has been confirmed by a larger sample of repeated measurements. While we did not place stars on multiple masks in the Wil 1 data set, the systematic error contribution is expected to be constant as this is the same spectrograph setup and velocity cross-correlation routines are identical. We add the random and systematic errors in quadrature to arrive at the final velocity error for each science measurement.

The fitted velocities were visually inspected to ensure the reliability of the fit. Radial velocities for 111 stars of the 423 objects targeted passed this visual inspection. For the rest of this paper, we only consider the 97 of those 111 stars that have

spectra with S/N > 2, and that have velocity uncertainties of less than 10 km s$^{-1}$. The median velocity uncertainty of these 97 stars is 3.5 km s$^{-1}$. The median velocity uncertainty in the subsample of those stars most likely to be Wil 1 members is 4.7 km s$^{-1}$, because the faintest of these 97 stars are dominated by MS stars belonging to Wil 1. All velocity histograms shown in this paper thus have a binsize of 4.7 km s$^{-1}$.

### 2.5. Comparing Relative and Deriving Absolute Abundances of Individual Stars

In Sections 3.3 and 3.4, we will use the relative stellar abundances imprinted on these spectra to identify likely bright member stars and to compare with stars observed by the SEGUE survey. In Section 4.1, we will then calculate the absolute [Fe/H] abundances of three bright member stars. We describe here the techniques used to measure those relative and absolute abundances.

To assess relative stellar abundances, we use the reduced equivalent width (EW, $W'$) of the Ca II lines. We utilize two functional forms of $W'$, one which has been calibrated for low metallicity stars (Starkenburg et al. 2010) and the standard (Rutledge et al. 1997) calibration. For both, we measure the CaT lines at 8498, 8542, and 8662 Å using the continuum and line definitions described in Rutledge et al. (1997) to calculate $\Sigma$Ca. We determine the uncertainty on $\Sigma$Ca with the Monte Carlo method described above. Added in quadrature to the Monte Carlo uncertainties is a systematic uncertainty of 0.25 Å, determined using the same method described in Simon & Geha (2007), but using a larger sample of repeated measurements.

Throughout the paper, we primarily report the value of the Rutledge et al. (1997) definition of $W'$ such that $\Sigma$Ca = $0.5\mathrm{EW}_{8498\,\text{Å}} + \mathrm{EW}_{8542\,\text{Å}} + 0.6\mathrm{EW}_{8662\,\text{Å}}$ and $W' = \Sigma\mathrm{Ca} - 0.64(V_{\mathrm{HB}} - V)$. $V$ is the $V$-band magnitude of each RGB star and $V_{\mathrm{HB}}$ is the magnitude of the horizontal branch. To obtain $V$, we convert our SDSS $g$- and $r$-band magnitudes into $V$ band using the photometric transformations given in Tables 1 and 2 of Blanton & Roweis (2007). The apparent $V$ magnitude of the one spectroscopically confirmed star in the flat part of Wil 1's horizontal branch is 18.45 mag. Although this approach minimizes assumptions, using a single star to determine $V_{\mathrm{HB}}$ introduces a possible offset into our $W'$ calculations; if the star is variable then its current apparent magnitude may not equal its average value. However, Siegel et al. (2008) found no RR Lyrae stars in Wil 1 in their time-series imaging of the object. Regardless, a small shift the $V_{\mathrm{HB}}$ we use to calculate $W'$ would not affect any conclusion of this paper.

We also use the metallicity calibration detailed in Starkenburg et al. (2010) to calculate [Fe/H] from $W'$, where $W'$ is defined as $0.43(V - V_{\mathrm{HB}}) + \Sigma\mathrm{Ca}_{(2+3)} - 2(\Sigma\mathrm{Ca}_{(2+3)}^{-1.5}) + 0.034(V - V_{\mathrm{HB}})$, and $\Sigma\mathrm{Ca}_{(2+3)} = \mathrm{EW}_{8542\,\text{Å}} + \mathrm{EW}_{8662\,\text{Å}}$. This study excluded the Ca II line at 8498 Å because it is the weakest of the three lines and has been shown to contribute more to the relative uncertainty than the two stronger lines (Armandroff & Da Costa 1991). The CaT–[Fe/H] relation presented in Starkenburg et al. (2010) was calibrated for RGB stars in the metallicity range $-4.0 <$ [Fe/H] $\sim -0.5$ and which lie within $-3 < (V - V_{\mathrm{HB}}) < 0$ or $-3 < (M_V) < 0.8$.

To derive the absolute abundances of bright member stars, we use the spectral synthesis method of Kirby et al. (2008a, hereafter KGS08). This method relies on comparing an observed medium-resolution spectrum with a grid of synthetic spectra covering a range of effective temperature ($T_{\mathrm{eff}}$), surface gravity

(log $g$), and composition. All of our spectra with high enough S/N for this technique are bright enough to be in the SDSS database, so we determine $V$ and $I$ for each star by transforming the SDSS $gri$ magnitudes with the relationship derived by Jordi et al. (2006). KGS08 found that uncertainty in the measured colors, ages, and alpha-abundances of stars does not substantially affect the estimated $T_{\mathrm{eff}}$ and log $g$. The best-matching composition is then found by minimizing residuals between the observed spectrum and a smoothed synthetic spectrum matched to the DEIMOS spectral resolution. To derive error bars on the best-matching [Fe/H], we calculate $\chi^2$ contours for every star by allowing both [Fe/H] and $T_{\mathrm{eff}}$ to vary. We separately varied $T_{\mathrm{eff}}$ by $\pm125$ K and 250 K and log $g$ by $\pm0.3$ dex and 0.6 dex. The surface gravity makes almost no difference in [Fe/H] because there are no visible ionized Fe lines in red giants in the observed spectral range. Changing $T_{\mathrm{eff}}$ by $\pm125$ K yields a $\delta$[Fe/H] of 0.13 dex and by an unrealistically large $\pm250$ K yields a $\delta$[Fe/H] of 0.26 dex for each star we study in this paper. KGS08 found that their technique measured [Fe/H] with 0.25 (0.5) dex accuracy on spectra of Galactic GC stars with S/N $\sim 20$ ($\sim 10$) Å$^{-1}$. The success of this method has been confirmed by a comparison with high-resolution abundances of over 100 stars in GCs, the halo field, dwarf galaxies, and of six RGB stars with $-3.3 <$ [Fe/H] $< -2.3$ in the ultra-faint dSphs (Kirby et al. 2008b, 2010).

## 3. A SPECTROSCOPIC SAMPLE OF WIL 1 STARS

To study the stellar population and kinematic properties of Wil 1, we need to identify a sample of member stars with minimal contamination from interlopers. Wil 1 lies at relatively high Galactic latitude $(l, b) = (158°.6, 56°.8)$. However, its systemic velocity is $\sim -12.3 \pm 2.5$ km s$^{-1}$ (Martin et al. 2007) and the median velocity of all Milky Way stars in the direction of Wil 1 is $-15.0$ km s$^{-1}$ using the Besancon Galaxy model[9] (Robin et al. 2003). In addition to overlapping in velocity, stars in Wil 1 have colors and magnitudes very similar to the colors and magnitudes of stars in the Milky Way's thick disk and halo.

In this section, we use color, magnitude, and velocity to select an initial sample of 45 Wil 1 candidate member stars. We then derive the predicted contamination from Milky Way foreground stars within this member sample. Finally, we identify 5 stars that are probable interlopers and present the properties of the remaining 40 probable Wil 1 member stars.

### 3.1. A Color–Magnitude–Velocity Sample of Wil 1 Candidate Stars

The first required criterion for Wil 1 membership is having a color and magnitude consistent with the stellar population of Wil 1. We use a loose CM selection, as shown by boxes overplotted with dotted lines in Figure 1. We used this loose cut, rather than proximity to a fiducial cluster sequence, to avoid making a priori assumptions about the stellar population of Wil 1. Fifty-eight of the 97 stars in our spectroscopic catalog satisfy these CM criteria.

The second required criterion for Wil 1 membership is a velocity consistent with belonging to Wil 1. Figure 2 shows the heliocentric velocity histogram of these 58 stars, along with the velocity histogram of the 39 stars that do not satisfy the CM selection for Wil 1 membership. The velocity distribution of the 58 CM-selected stars is strongly peaked, with 45 stars between $-30$

---
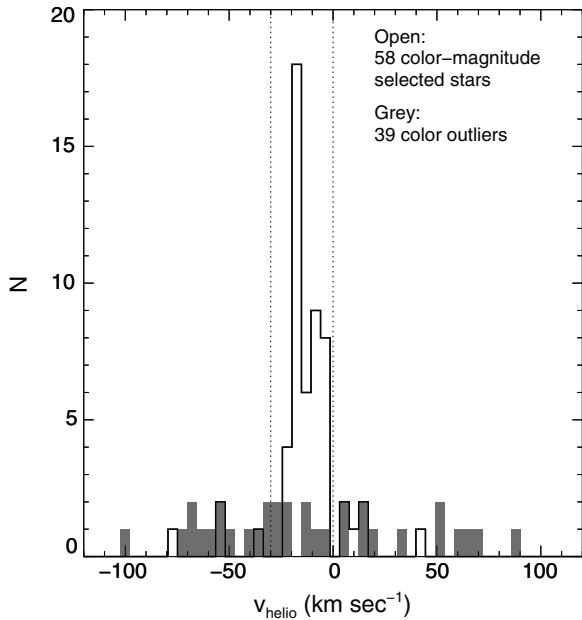
**Figure 2.** Velocity distributions of the 58 stars that satisfy our Wil 1 color–magnitude selection criteria (open) and the 39 stars that do not satisfy these criteria (gray filled). The dotted lines show the velocity range of $-30$ km s$^{-1}$ < $v_{\rm helio}$ < 0 km s$^{-1}$ used to select Wil 1 member stars. Binsize is 4.7 km s$^{-1}$, the median velocity error of the 58 stars passing the color–magnitude criteria for membership.
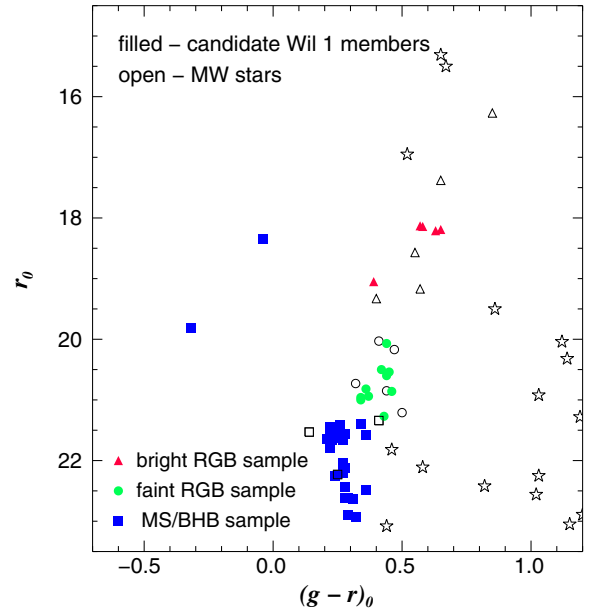


**Figure 3.** Color–magnitude diagram of the 97 stars with DEIMOS/Keck velocities. Open symbols show Milky Way stars. Filled symbols show probable Wil 1 member stars, as selected by color–magnitude and velocity ($-30$ km s$^{-1}$ < $v$ < 0 km s$^{-1}$) criteria. Triangles, circles, and squares highlight stars belonging to the bRGB, fRGB, and MS/BHB subsamples used to characterize foreground contamination. Five-point stars show those stars that did not satisfy the initial color–magnitude cut for membership.

(A color version of this figure is available in the online journal.)

and 0 km s$^{-1}$. We identify these 45 color–magnitude–velocity (CM–V) selected stars as likely Wil 1 members. This does not necessarily mean that none of the 13 CM selected stars with outlying velocities are physically associated with Wil 1. However, the spatial distribution of those 13 stars at outlying velocities is not clustered around the Wil 1 center.

We present in Table 2 the equatorial coordinates, $r$ magnitudes, $g - r$ colors, heliocentric velocities, and spectral S/N of the 45 CM–V selected Wil 1 member stars. We also include the CaT $W'$ (and uncertainty) for the 15 possible RGB, as calculated in Section 2.5. Table 3 contains the same data (but not $W'$) for the 52 non-member stars.

### 3.2. Predicting the Number of Interlopers in the Color–Magnitude–Velocity Sample

Figure 3 shows a CMD of the stars in our spectroscopic catalog. Filled symbols represent the 45 candidate Wil 1 members selected in Section 3.1, and open symbols represent the 52 foreground Milky Way stars. The number of open symbols overlapping with the filled symbols shows that 40% of stars with colors and magnitudes consistent with the RGB of Wil 1 are foreground stars belonging to the Milky Way. These foreground stars were only identified because their line-of-sight velocities were different than those of Wil 1 stars. The median velocity of Milky Way stars passing the CM criterion for membership is $-35.7$ km s$^{-1}$ (based on the Besancon Galaxy model), with 16% of these having $-30$ km s$^{-1}$ < $v_{\rm los}$ < 0 km s$^{-1}$. How many Milky Way interlopers remain in the CM–V sample of 45 candidate Wil 1 members?

We simulate the number of interloper stars expected among the 45 candidate members using the Besancon Galaxy model. Because photometric studies suggest the presence of tidal features around Wil 1 (Willman et al. 2006; Martin et al. 2007), we first predict the number of Milky Way contaminant stars without assuming that all CM-selected stars outside the Wil 1

velocity peak belong to the Milky Way. We instead use the Besancon model to predict the absolute number density of Milky Way stars satisfying the CM–V criteria for candidate members. The predicted number of contaminant stars thus rests on the assumptions that the velocity distribution of Besancon model stars and the absolute numbers of stars in the Besancon model are correct. We later verify that this yields a reasonable prediction.

The primary ingredients in our calculation are the following:

1. $n_{\rm fg,vel}$, the projected number density of Milky Way stars in the Besancon model satisfying the CM–V criteria for Wil 1 membership. We calculated $n_{\rm fg,vel}$ and its dispersion in 1000 small fields randomly placed in a 1 deg$^2$ Besancon simulation centered on the position of Wil 1. To do this, we shuffled the right ascensions and declinations of Besancon model stars before selecting each random field. The random fields each had an area approximately equal to that of our spectroscopic survey footprint. Because the CM cuts applied to our data were liberal, we simply used the model Canada–France–Hawaii Telescope-Megacam $g$ and $r$ magnitudes as a proxy for the observed SDSS $g$ and $r$ magnitudes. We convolved 4.7 km s$^{-1}$ measurement uncertainties, the median for the 45 candidate members, to the model velocities of each Besancon star. The average number of possible interlopers in the CM–V sample within a given area of sky, $A$, is then $N_{\rm cont,vel} = A * n_{\rm fg,vel}$.

2. $f_{\rm targ}$, the fraction of stars in our photometric catalog satisfying the CM criteria for Wil 1 membership that also end up in our spectroscopic catalog of 97 stars. Not all stars satisfying the CM criteria for membership were targeted, and not all targeted stars had spectra with high enough S/N to be in the final spectroscopic catalog. To derive the true number of Milky Way interlopers, $N_{\rm cont,vel}$ needs to be multiplied

**Table 2**
Data for the 45 Candidate Willman 1 Members

| ID | $\alpha$ (J2000) (h m s) | $\delta$ (J2000) (° ′ ″) | $r$ (mag) | $(g-r)$ (mag) | $v_{\mathrm{helio}}$ ( km s$^{-1}$) | S/N | CaT EW (Å) |
|----|----|----|----|----|----|----|----|
| 1 | 10 49 18.06 | +51 02 16 | 18.13 | 0.57 | $-5.4 \pm 2.2$ | 84.1 | $1.63 \pm 0.41$ |
| 2 | 10 49 52.51 | +51 03 42 | 18.14 | 0.58 | $-18.5 \pm 2.2$ | 85.5 | $1.41 \pm 0.41$ |
| 3[a] | 10 49 42.87 | +51 04 22 | 18.19 | 0.65 | $-13.3 \pm 2.2$ | 88.1 | $4.24 \pm 0.39$ |
| 4[a] | 10 49 12.40 | +51 05 43 | 18.21 | 0.63 | $-7.4 \pm 2.2$ | 72.3 | $4.65 \pm 0.41$ |
| 5 | 10 49 07.79 | +50 56 50 | 18.35 | $-0.04$ | $-11.1 \pm 2.7$ | 34.3 | . . . |
| 6[a] | 10 49 48.53 | +51 00 32 | 19.05 | 0.39 | $-2.1 \pm 2.4$ | 21.6 | $3.65 \pm 0.46$ |
| 7 | 10 49 13.13 | +51 02 32 | 19.81 | $-0.32$ | $-18.2 \pm 6.8$ | 18.5 | . . . |
| 8 | 10 49 17.41 | +51 03 25 | 20.07 | 0.44 | $-9.4 \pm 3.6$ | 9.4 | $1.39 \pm 0.46$ |
| 9 | 10 49 10.11 | +51 03 00 | 20.50 | 0.42 | $-13.1 \pm 3.0$ | 16.3 | $2.38 \pm 0.40$ |
| 10[a] | 10 49 15.95 | +51 02 26 | 20.54 | 0.45 | $-8.9 \pm 3.9$ | 9.8 | $4.46 \pm 0.41$ |
| 11[a] | 10 49 24.97 | +51 09 23 | 20.60 | 0.44 | $-4.9 \pm 2.7$ | 16.8 | $4.51 \pm 0.39$ |
| 12 | 10 49 21.14 | +51 03 29 | 20.82 | 0.36 | $-5.6 \pm 5.1$ | 5.6 | $0.75 \pm 0.44$ |
| 13 | 10 48 58.10 | +51 02 53 | 20.86 | 0.46 | $-3.8 \pm 2.7$ | 8.3 | $2.79 \pm 0.40$ |
| 14 | 10 49 40.82 | +51 03 39 | 20.94 | 0.37 | $-18.9 \pm 3.7$ | 15.3 | $2.60 \pm 0.40$ |
| 15 | 10 49 30.94 | +51 03 40 | 20.96 | 0.34 | $-16.4 \pm 3.9$ | 13.2 | $2.21 \pm 0.41$ |
| 16 | 10 49 16.75 | +51 04 03 | 21.00 | 0.34 | $-7.6 \pm 3.2$ | 10.6 | $3.69 \pm 0.44$ |
| 17 | 10 50 02.85 | +51 02 32 | 21.27 | 0.43 | $-15.8 \pm 5.1$ | 5.4 | $3.12 \pm 0.41$ |
| 18 | 10 50 19.29 | +51 00 12 | 21.39 | 0.34 | $-24.2 \pm 2.7$ | 7.5 | . . . |
| 19 | 10 48 57.12 | +51 02 31 | 21.42 | 0.26 | $-15.3 \pm 3.9$ | 7.3 | . . . |
| 20 | 10 49 28.06 | +51 01 51 | 21.45 | 0.22 | $-21.2 \pm 3.1$ | 3.5 | . . . |
| 21 | 10 49 28.06 | +51 01 51 | 21.45 | 0.22 | $-12.9 \pm 4.6$ | 3.4 | . . . |
| 22 | 10 49 12.55 | +51 03 05 | 21.49 | 0.25 | $-15.9 \pm 5.3$ | 7.0 | . . . |
| 23 | 10 49 26.31 | +51 03 16 | 21.49 | 0.22 | $-10.5 \pm 6.7$ | 8.5 | . . . |
| 24 | 10 49 25.06 | +51 02 52 | 21.54 | 0.25 | $-13.7 \pm 5.1$ | 4.6 | . . . |
| 25 | 10 49 07.67 | +51 01 46 | 21.56 | 0.23 | $-19.1 \pm 7.2$ | 6.9 | . . . |
| 26 | 10 48 44.41 | +51 02 06 | 21.57 | 0.28 | $-18.4 \pm 4.7$ | 7.3 | . . . |
| 27 | 10 49 51.52 | +51 01 52 | 21.58 | 0.36 | $-16.0 \pm 3.5$ | 8.3 | . . . |
| 28 | 10 49 34.77 | +51 04 28 | 21.60 | 0.27 | $-18.9 \pm 8.8$ | 7.2 | . . . |
| 29 | 10 49 09.93 | +51 00 56 | 21.63 | 0.26 | $-4.8 \pm 5.0$ | 6.4 | . . . |
| 30 | 10 49 29.73 | +51 02 58 | 21.64 | 0.21 | $-23.5 \pm 3.7$ | 6.1 | . . . |
| 31 | 10 49 54.69 | +51 03 27 | 21.66 | 0.27 | $-8.0 \pm 4.8$ | 4.0 | . . . |
| 32 | 10 49 14.23 | +51 01 10 | 21.66 | 0.23 | $-10.5 \pm 4.8$ | 7.6 | . . . |
| 33 | 10 49 27.64 | +51 03 32 | 21.75 | 0.22 | $-3.6 \pm 4.8$ | 3.8 | . . . |
| 34 | 10 49 05.17 | +51 01 42 | 21.80 | 0.22 | $-14.8 \pm 4.9$ | 6.6 | . . . |
| 35 | 10 49 22.53 | +51 05 47 | 22.04 | 0.27 | $-23.7 \pm 9.2$ | 2.4 | . . . |
| 36 | 10 49 11.98 | +51 03 04 | 22.13 | 0.28 | $-19.3 \pm 7.8$ | 3.1 | . . . |
| 37 | 10 49 02.81 | +50 59 40 | 22.20 | 0.27 | $-19.7 \pm 6.5$ | 4.8 | . . . |
| 38 | 10 49 40.69 | +51 04 19 | 22.26 | 0.24 | $-17.1 \pm 5.0$ | 4.4 | . . . |
| 39 | 10 49 14.93 | +51 02 53 | 22.44 | 0.28 | $-10.0 \pm 4.6$ | 3.6 | . . . |
| 40 | 10 49 13.44 | +51 02 43 | 22.48 | 0.36 | $-5.6 \pm 9.0$ | 3.1 | . . . |
| 41 | 10 49 10.91 | +51 02 14 | 22.61 | 0.29 | $-19.7 \pm 7.4$ | 2.3 | . . . |
| 42 | 10 49 47.62 | +51 02 03 | 22.62 | 0.28 | $-18.1 \pm 8.6$ | 3.5 | . . . |
| 43 | 10 48 54.03 | +51 01 38 | 22.63 | 0.31 | $-16.1 \pm 5.6$ | 3.1 | . . . |
| 44 | 10 49 40.22 | +51 03 04 | 22.89 | 0.29 | $-9.5 \pm 5.5$ | 2.9 | . . . |
| 45 | 10 49 10.96 | +51 01 32 | 22.93 | 0.32 | $-16.9 \pm 6.4$ | 2.4 | . . . |

**Notes.** S/N is the median per pixel signal to noise for each star. Velocity error bars were determined from measurement overlaps as discussed in Section 2.4. We supply the CaT EW only for stars possibly in the fRGB or bRGB populations of Wil 1.

[a] Star flagged as a likely non-member by the CaT EW < 2.3 Å or color criterion described in Section 3.3.

by $f_{\mathrm{targ}}$. Because both the density of stars and the fraction of sky covered by observations decrease with increasing Wil 1 distance, $f_{\mathrm{targ}}$ is a function of distance from the center of Wil 1. We thus calculate $f_{\mathrm{targ}}$ in each of three distance ranges: 0–2 $r_{\mathrm{half}}$, 2–4 $r_{\mathrm{half}}$, and 4–6 $r_{\mathrm{half}}$.

The contamination in the Wil 1 candidate member sample is expected to be primarily composed of stars belonging to the Milky Way's thick disk and halo. Because the relative number of thick disk and halo stars varies across the CMD (thick disk stars dominate at brighter apparent magnitudes, halo stars at fainter) and because these two galaxy components have different

velocity distributions, $n_{\mathrm{fg,vel}}$ is a function of apparent magnitude. Because stars were prioritized by apparent magnitude in target selection, $f_{\mathrm{targ}}$ is also a function of apparent magnitude. We therefore separately estimate the foreground contamination in three subsets of the Wil 1 population: (1) the five relatively bright red giant branch (bRGB; $r_0 < 19.5$ mag), (2) the 10 faint red giant branch (fRGB; 19.5 mag $< r_0 < 21.3$ mag), and (3) the 30 MS and blue horizontal branch (BHB) stars.

The left panel of Figure 4 shows $f_{\mathrm{targ}}$ as a function of distance from Wil 1 for the bRGB, fRGB, and MS/BHB subsamples. The overall target efficiency at all distances is much lower than one, because many stars at the faint end of our acceptable magnitude

range ($r_0 = 23$) for target selection were not measured with high enough S/N for a robust velocity to be extracted. Many stars remain to be observed in the center of Wil 1 if such faint magnitudes can be reached. The target efficiency for fRGB stars remains high out to large distances from Wil 1, even though our fractional spatial coverage beyond $3r_{half}$ is quite low. This is because our mask placement included two out of the six total stars between 4 and $6r_{half}$ that are consistent with the fRGB of Wil 1. Although target efficiency is low at large $d$, only 4% of stars are expected to lie beyond three elliptical half-light radii of a system well-described by an exponential profile (see also Section 4.2).

The average expected number of contaminant stars in each of the bRGB, fRGB, and MS/BHB CM–V subsamples in each annulus is

$$N_{cont,vel} = f_{targ} \times A_{annulus} \times n_{fg,vel}, \quad (1)$$

and the average dispersion in this number is

$$\sigma_{cont,vel} = f_{targ} \times A_{annulus} \times \sigma_{fg,vel}, \quad (2)$$

where $A_{annulus}$ is the area of each elliptical annulus, and $f_{targ}$, $n_{fg,vel}$, and $\sigma_{fg,vel}$ are calculated separately for each of the bRGB, fRGB, and MS/BHB subpopulations. We predict a fraction of one interloper star within each of the three subpopulations within each of the three annuli. The probability that any individual star is an interloper increases with distance and is shown in the bottom left panel of Figure 4.

We sum the predicted average numbers (and dispersions, in quadrature) of interlopers in each annulus to derive the average total numbers (and dispersions) of interloper stars expected in each of the bRGB, fRGB, and MS/BHB subsamples and find $1.5 \pm 1.0$, $0.7 \pm 0.5$, and $0.6 \pm 0.3$ stars, respectively. Although the number of stars in our sample increases at fainter apparent magnitudes, the number of expected contaminants is low in the 30 possible MS members. This small predicted contamination results from the low overall target efficiency combined with the large number of Wil 1 stars in its MS relative to its bRGB and fRGB. To convert these fractional numbers of stars into a physical number of stars that may be in our sample, we used the IDL function POIDEV to generate $10^5$ Poisson random deviates with the predicted mean and dispersion in the number of interloper stars. The result of this simulation is shown in the right panel of Figure 4. 50% of all trials contained one or zero predicted interlopers among the entire candidate sample of 45 stars—one RGB star. 90% of all trials had seven or fewer interlopers (three bRGB, two fRGB, and two MS/BHB).

To sanity check this prediction, we also use the above method to predict the number of Milky Way stars expected in our data set outside the velocity cut for membership in our original CM-selected sample. At 50% (90%) confidence, the number of stars with $v < -30$ km s$^{-1}$ or $v > 0$ km s$^{-1}$ we predict to be in the bRGB, fRGB, and MS/HB regions of our spectroscopic data set are $\leqslant 5$, 4, and 4 (8, 7, and 7), respectively. Figure 3 shows that there are actually 5, 5, and 3 stars with $v < -30$ km s$^{-1}$ or $v > 0$ km s$^{-1}$ in the RGB, fRGB, and MS/HB regions of our spectroscopic data set. Our technique thus accurately predicts the number of stars in our spectroscopic catalog at outlying velocities.

We also use a simpler technique that does not rely on the absolute calibration of the Besancon model to predict the number of interloper stars among the 45 candidate members. This "scaled histogram" approach instead relies on assuming

**Table 3**
Data for the 52 Milky Way Foreground Stars in Our Sample

| ID | $\alpha$ (J2000) (h m s) | $\delta$ (J2000) (° ′ ″) | $r$ (mag) | $(g-r)$ (mag) | $v_{helio}$ ( km s$^{-1}$) | S/N |
|---|---|---|---|---|---|---|
| 46 | 10 50 15.74 | +51 02 22 | 15.31 | 0.65 | $-24.4 \pm 2.2$ | 227.1 |
| 47 | 10 49 09.55 | +50 54 53 | 15.50 | 0.67 | $16.7 \pm 2.3$ | 220.2 |
| 48 | 10 49 07.46 | +51 04 06 | 16.27 | 0.85 | $6.4 \pm 2.2$ | 172.9 |
| 49 | 10 48 38.69 | +51 00 26 | 16.95 | 0.52 | $-119.7 \pm 2.2$ | 132.6 |
| 50 | 10 49 54.92 | +51 00 40 | 17.38 | 0.65 | $-53.8 \pm 2.2$ | 87.8 |
| 51 | 10 49 27.20 | +50 59 26 | 18.57 | 0.55 | $155.1 \pm 2.3$ | 43.3 |
| 52 | 10 48 45.47 | +50 58 40 | 19.17 | 0.57 | $-171.9 \pm 2.3$ | 37.0 |
| 53 | 10 48 47.90 | +50 57 17 | 19.33 | 0.40 | $14.8 \pm 2.3$ | 34.4 |
| 54 | 10 49 13.10 | +51 06 26 | 19.50 | 0.86 | $-24.5 \pm 2.6$ | 19.0 |
| 55 | 10 50 02.13 | +51 02 04 | 19.62 | 1.26 | $-29.5 \pm 2.2$ | 47.5 |
| 56 | 10 49 21.51 | +51 08 26 | 20.03 | 1.42 | $13.2 \pm 2.2$ | 78.3 |
| 57 | 10 50 19.02 | +50 59 18 | 20.03 | 0.41 | $-249.3 \pm 2.4$ | 20.3 |
| 58 | 10 50 13.69 | +51 00 06 | 20.04 | 1.12 | $-205.0 \pm 2.3$ | 23.3 |
| 59 | 10 49 12.90 | +51 06 17 | 20.17 | 0.47 | $14.3 \pm 2.4$ | 18.4 |
| 60 | 10 49 28.48 | +51 01 33 | 20.27 | 1.41 | $-23.3 \pm 2.3$ | 24.6 |
| 61 | 10 48 55.77 | +51 01 19 | 20.32 | 1.14 | $-157.8 \pm 2.5$ | 26.4 |
| 62 | 10 50 05.69 | +51 01 54 | 20.33 | 1.40 | $-10.7 \pm 2.2$ | 28.7 |
| 63 | 10 49 56.07 | +51 00 00 | 20.61 | 1.40 | $6.2 \pm 2.2$ | 24.0 |
| 64 | 10 49 22.03 | +50 59 05 | 20.73 | 0.32 | $-36.3 \pm 3.6$ | 8.2 |
| 65 | 10 49 20.02 | +51 04 58 | 20.83 | 1.35 | $60.7 \pm 2.3$ | 31.3 |
| 66 | 10 49 34.57 | +51 02 39 | 20.85 | 0.44 | $-52.8 \pm 4.8$ | 7.9 |
| 67 | 10 49 13.34 | +51 04 28 | 20.85 | 1.39 | $-21.9 \pm 2.3$ | 14.7 |
| 68 | 10 49 37.15 | +51 02 37 | 20.92 | 1.03 | $-69.5 \pm 2.4$ | 15.0 |
| 69 | 10 50 09.54 | +50 59 22 | 21.06 | 1.33 | $-205.3 \pm 2.4$ | 14.6 |
| 70 | 10 50 11.50 | +51 01 11 | 21.21 | 0.50 | $39.9 \pm 3.8$ | 6.5 |
| 71 | 10 49 39.43 | +51 02 03 | 21.28 | 1.19 | $-69.1 \pm 2.3$ | 31.3 |
| 72 | 10 49 31.01 | +51 01 33 | 21.34 | 0.41 | $-78.9 \pm 4.0$ | 10.3 |
| 73 | 10 49 53.75 | +51 00 43 | 21.35 | 1.37 | $-52.2 \pm 2.3$ | 14.9 |
| 74 | 10 49 03.74 | +51 00 38 | 21.38 | 1.32 | $-49.0 \pm 2.5$ | 18.1 |
| 75 | 10 49 13.88 | +51 05 12 | 21.47 | 1.40 | $-14.7 \pm 3.0$ | 7.9 |
| 76 | 10 49 03.41 | +51 00 48 | 21.53 | 0.14 | $7.4 \pm 5.2$ | 6.8 |
| 77 | 10 49 21.25 | +51 09 48 | 21.79 | 1.33 | $-100.1 \pm 2.4$ | 19.2 |
| 78 | 10 49 52.91 | +51 03 14 | 21.80 | 1.30 | $-37.9 \pm 3.2$ | 6.7 |
| 79 | 10 48 48.74 | +51 03 16 | 21.82 | 0.46 | $65.9 \pm 4.7$ | 6.3 |
| 80 | 10 49 07.25 | +51 02 12 | 21.87 | 1.44 | $50.6 \pm 2.4$ | 22.9 |
| 81 | 10 49 30.19 | +51 07 23 | 21.90 | 1.34 | $-59.7 \pm 4.3$ | 15.4 |
| 82 | 10 49 06.01 | +51 02 51 | 22.11 | 0.58 | $68.1 \pm 8.8$ | 4.2 |
| 83 | 10 49 15.36 | +51 01 05 | 22.15 | 1.50 | $-41.4 \pm 2.5$ | 24.1 |
| 84 | 10 49 14.03 | +51 08 44 | 22.22 | 1.30 | $-4.9 \pm 4.4$ | 6.4 |
| 85 | 10 49 15.46 | +51 05 51 | 22.23 | 1.35 | $-73.4 \pm 2.6$ | 18.3 |
| 86 | 10 49 20.72 | +51 01 41 | 22.23 | 0.25 | $8.7 \pm 7.2$ | 3.5 |
| 87 | 10 49 39.60 | +51 02 26 | 22.25 | 1.03 | $87.3 \pm 5.3$ | 16.6 |
| 88 | 10 49 24.43 | +51 09 14 | 22.38 | 1.40 | $50.4 \pm 2.6$ | 15.3 |
| 89 | 10 50 14.71 | +50 59 46 | 22.42 | 0.82 | $-32.9 \pm 7.1$ | 3.4 |
| 90 | 10 49 24.62 | +51 07 56 | 22.56 | 1.02 | $32.9 \pm 3.3$ | 7.9 |
| 91 | 10 48 54.87 | +51 00 07 | 22.57 | 1.49 | $-54.4 \pm 3.4$ | 21.2 |
| 92 | 10 49 30.07 | +51 08 19 | 22.61 | 1.25 | $-65.2 \pm 3.5$ | 8.0 |
| 93 | 10 50 14.66 | +51 02 16 | 22.61 | 1.39 | $19.8 \pm 6.4$ | 5.1 |
| 94 | 10 50 07.85 | +51 02 07 | 22.77 | 1.29 | $-200.9 \pm 5.0$ | 6.7 |
| 95 | 10 49 05.30 | +51 00 24 | 22.89 | 1.20 | $124.3 \pm 4.7$ | 12.1 |
| 96 | 10 48 57.47 | +50 57 54 | 23.05 | 1.15 | $-10.0 \pm 3.1$ | 9.2 |
| 97 | 10 49 38.33 | +51 01 38 | 23.08 | 0.44 | $5.7 \pm 7.8$ | 2.1 |

**Notes.** S/N is the median per pixel signal to noise for each star. Velocity error bars were determined from measurement overlaps as discussed in Section 2.4.

that the 13 bRGB, fRGB, and MS/HB-colored stars at outlying velocities are all Milky Way foreground stars. Treating each of these three regions of the CMD separately, we determine the relative numbers of Milky Way stars in the Besancon model with velocities inside and outside the velocity cut for membership and apply this scaling factor to the numbers of stars we observe outside the velocity cut for membership. We use these fractional
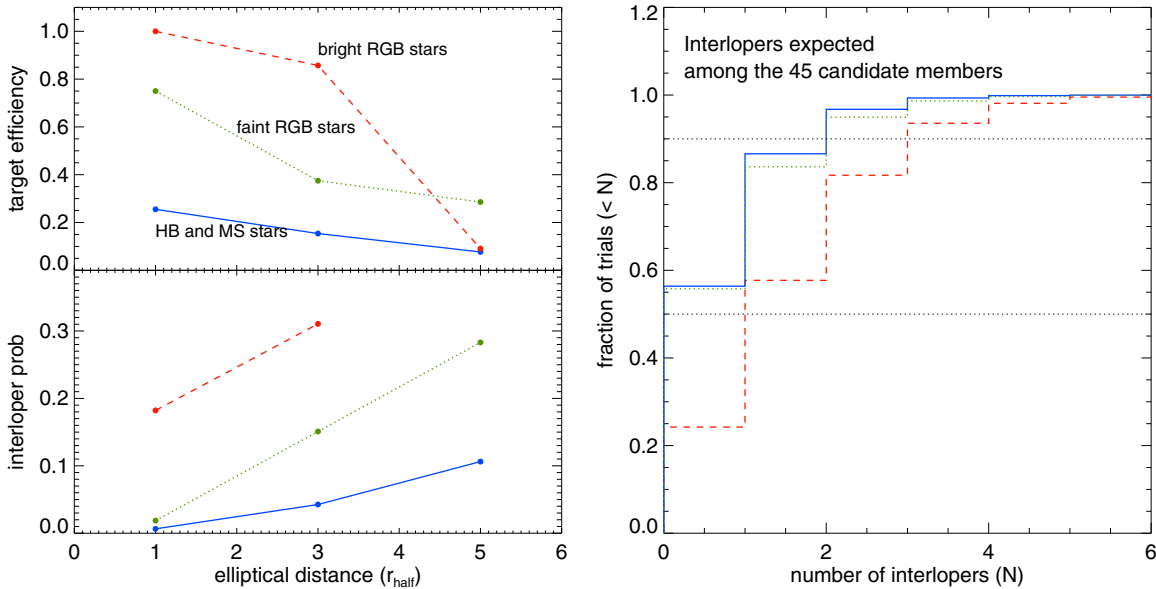
**Figure 4.** Left panel, top: the fraction of all stars, as a function of elliptical distance from the Wil 1 center, that pass color–magnitude criteria for Wil 1 membership and also end up in our final spectroscopic sample with well-measured velocities. This target efficiency is shown for three different subpopulations of Wil 1 stars—bRGB candidates, fRGB candidates, and BHB/MS candidates. Left panel, bottom: the probability that any individual star is an interloper, as a function of distance. Right panel: the predicted number of Milky Way interlopers in the sample of 45 candidate members in $10^5$ Poisson realizations of the foreground. Color coding is the same as the left panel. 90% of all trials had seven or fewer interlopers (three bRGB, two fRGB, and two MS/BHB).
(A color version of this figure is available in the online journal.)

**Table 4**
Predicted Number of Milky Way Stars in the Sample of 45 Candidate Members

| Subsample | Observed | Predicted Interlopers | |
| --- | --- | --- | --- |
| | | Simulation 50% (90%) Confidence | Scaled Histogram 50% (90%) Confidence |
| bRGB | 5 | $\leqslant 1$ (3) | $\leqslant 1$ (3) |
| fRGB | 10 | $\leqslant 0$ (2) | $\leqslant 1$ (2) |
| MS/BHB | 30 | $\leqslant 0$ (2) | $\leqslant 0$ (2) |

**Notes.** The two methods for predicting the Milky Way contamination are described in Section 3.2. It was calculated both with a simulation based on the Besancon Galaxy model and by scaling the histogram of the number of stars at velocities inconsistent with membership.

numbers of stars to generate $10^5$ Poisson realizations of the predicted number of bRGB, fRGB, and MS/HB interlopers and find that 50% (90%) of trials contain $\leqslant$ 1, 1, and 0 (3, 2, and 2) interlopers, respectively. This technique thus yields very similar results as the full simulations, predicting a median of only two interlopers, with fewer than or equal to seven at 90% confidence.

We summarize these predictions for interlopers among the 45 candidate members in Table 4.

### 3.3. Identifying Interloper Stars in Wil 1 Sample

The calculations in Section 3.2 revealed that we expect 1–7 Milky Way interlopers among the 45 Wil 1 candidate stars identified in Section 3.1. When broken down by subsets of stellar population, we predict 1–3 interlopers among the 5 bRGB candidates, 0–2 interlopers among the 10 fRGB candidates, and 0–2 interlopers among the 30 MS/HB candidates. We now attempt to identify these interlopers. Because the fractional contamination of the candidate MS/HB Wil 1 members is small compared to that of RGB stars, and because we do not have a reasonable spectroscopic [Fe/H] indicator for the MS/HB

candidates, we only look for the 1–5 interlopers with RGB magnitudes and colors.

We use CaT reduced EW, $W'$ (calculated using the Rutledge definition described in Section 2.5), to flag possible interlopers. All recent spectroscopic studies of Milky Way dwarf galaxies use some metallicity indicator to select member stars (e.g., Walker et al. 2009). This selection means that the abundance spread we will infer for Wil 1 in Section 4.1 is necessarily a lower limit. We choose not to use velocity and position information to perform a likelihood analysis for member selection. We will show evidence that Wil 1 is both spatially and kinematically disturbed in Sections 4.2 and 5.2. We therefore do not want to assert that Wil 1 stars follow an exponential spatial distribution and Gaussian velocity distribution when discriminating member stars from interlopers.

Figure 5 shows $W'$ of the 15 candidate Wil 1 RGB stars as a function of $r_0$ magnitude. This figure shows a large spread of $W'$, with a big gap between the more metal-poor and more metal-rich stars at bright magnitudes. Given the gap at bright magnitudes, we hypothesize that the four higher $W'$ (more metal-rich) stars on this figure are possible foreground stars. The dotted line at $W' = 3.9$ Å in Figure 5 shows our adopted separation between possible foreground dwarfs and Wil 1 members. Using this $W'$ cut, there are four likely foreground RGB stars (Stars 3, 4, 10, and 11 in Table 2).

The fainter stars in Figure 5 do not show the same bi-modal distribution of $W'$ as the brighter stars. However, we adopt a cut at $W' = 3.9$ Å as a reasonable way to flag possible interlopers because (1) in Section 3.4 we will provide additional support for an interloper classification of Stars 3 and 4 and (2) we will show that this specific $W'$ cut impacts neither our conclusions about the classification of Wil 1 nor our conclusions about the kinematic properties of Wil 1.

We test this $W'$ cut by considering in detail the two brightest stars flagged as interlopers. One of these stars, Star 4, has a high-resolution Hobby Eberly Telescope (HET) spectrum from

**Table 5**
Additional Data for Bright Candidate Willman 1 Red Giants

| ID | Other ID[a] | $u_0$[b] | $g_0$ | $r_0$ | $i_0$ | $z_0$ | $v_{r,Martin}$ km s$^{-1}$[c] | [Fe/H][d] |
|----|----|----|----|----|----|----|----|----|
| 1 | . . . | $19.99 \pm 0.04$ | $18.66 \pm 0.02$ | $18.12 \pm 0.02$ | $17.87 \pm 0.02$ | $17.72 \pm 0.02$ | . . . | $-1.73 \pm 0.12$ |
| 2 | 1578 | $19.91 \pm 0.05$ | $18.69 \pm 0.02$ | $18.13 \pm 0.02$ | $17.85 \pm 0.02$ | $17.74 \pm 0.02$ | $-22.0 \pm 0.6$ | $-2.65 \pm 0.12$ |
| 3 | 1496 | $20.53 \pm 0.06$ | $18.81 \pm 0.02$ | $18.16 \pm 0.02$ | $17.92 \pm 0.02$ | $17.80 \pm 0.02$ | $-13.2 \pm 1.0$ | . . . |
| 4 | 1269 | $20.52 \pm 0.05$ | $18.84 \pm 0.02$ | $18.19 \pm 0.02$ | $17.98 \pm 0.02$ | $17.90 \pm 0.02$ | $-10.2 \pm 1.2$ | . . . |
| 6 | . . . | $20.65 \pm 0.06$ | $19.39 \pm 0.03$ | $19.02 \pm 0.02$ | $18.87 \pm 0.02$ | $18.85 \pm 0.04$ | . . . | . . . |

**Notes.** Stars 1 and 6 were neither in Siegel et al. (2008) nor in Martin et al. (2007).
[a] ID from Siegel et al. (2008).
[b] These magnitudes are all extinction corrected PSF magnitudes from SDSS Data Release 7 (Abazajian & Sloan Digital Sky Survey 2009) so differ slightly from the magnitudes quoted in Table 2.
[c] The velocities measured by Martin et al. (2007).
[d] Derived using the technique described in KGS08.
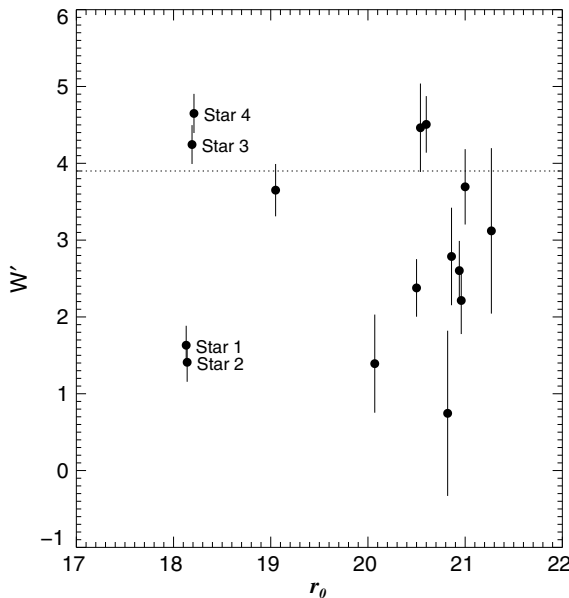


**Figure 5.** Reduced equivalent widths (Rutledge definition) of the calcium triplet feature measured for the 15 candidate Wil 1 member stars brighter than the base of the red giant branch. This figure shows a large spread in $W'$, with a gap between the more metal-rich and more metal-poor stars at the brightest magnitudes. Overplotted is a line at 3.9 Å, our subjective $W'$ cut between probable members and possible interloper stars.

Siegel et al. (2008). They could not obtain a consistent solution for Fe I and Fe II abundances under the assumption that this star was a giant. They argue that it is likely to be a foreground dwarf, consistent with our classification. Star 3 has $W'$ and SDSS colors very similar to that of Star 4 (see Tables 2 and 5). We thus consider it likely that Star 3 is also a foreground star, although this statement is not conclusive. Martin et al. (2007) also classified Star 3 as an interloper.

In addition to the four relatively high $W'$ stars, we classify the star with $r \sim 19$ and $W' \sim 3.2$ (Star 6 in Table 2) as an interloper. Figure 3 shows that Star 6 ($g - r = 0.39$) lies blueward of the main bRGB locus in $g - r$, despite its intermediate $W'$. For Star 6 to reasonably be part of Wil 1's stellar population, it would need to be quite metal-poor (inconsistent with its intermediate $W'$) to explain its blue color. Star 6 is thus a likely non-member, bringing the total number of stars flagged as contaminants on the RGB to 5 out of 15, which is at the upper edge of our contamination estimates.

To facilitate the reader reaching her own conclusions about the classification of the five brightest Wil 1 RGB candidate members, the SDSS de-reddened *ugriz* magnitudes of these stars are compiled in Table 5. To facilitate the reader's comparison with earlier spectroscopic studies of Wil 1, we also include the star IDs used by Siegel et al. (2008) and the velocities used by Martin et al. (2007) in this table.

While we cannot rule out the possibility that there are relatively metal-rich stars in Wil 1, we have outlined a reasonable approach to flagging likely RGB non-members. We exclude these five stars from our primary analysis in the remainder of this paper.

### 3.4. A Close Look at the Membership Probability of Stars 1 and 2

There is an abundance of circumstantial evidence for a member classification for both Stars 1 and 2. In their high-resolution HET spectroscopic study, Siegel et al. (2008) concluded that Star 2 (unlike Star 4) is a Wil 1 member giant. Star 1's photometric and spectroscopic properties are very similar to that of Star 2, providing some evidence that they both are true member stars. The positions and velocities of Stars 1 and 2 are both typical of those of the other 43 candidate member stars: Star 1 is only 0.6 projected half-light radii from the center of Wil 1 and has a heliocentric velocity of $-5.4 \pm 2.2$ km s$^{-1}$. 13% of the candidate members have more positive velocities than Star 1. Star 2 is 2.1 projected half-light radii from the center of Wil 1 and has a heliocentric velocity of $-18.5 \pm 2.2$ km s$^{-1}$. 27% of the candidate members lie at greater distance and 22% at more negative velocities. (We discuss this large velocity spread and the correlation between distance and velocity in Section 5.) We have also shown it to be unlikely that we have missed any foreground contaminants in the part of Wil 1's RGB that includes Stars 1 and 2.

We proceed with caution and now independently test the hypothesis that Star 1 or Star 2 may be a Milky Way halo star. We will show that Star 1's [Fe/H] is $-1.73 \pm 0.12$, similar to the peak of the halo's metallicity distribution function (Ryan & Norris 1991). We will then argue that Wil 1 is a dwarf galaxy, or remnant thereof, based on the [Fe/H] spread between Stars 1 and 2. This classification of Wil 1 thus hinges on the membership of both Stars 1 and 2.

We use the SEGUE survey database (Yanny et al. 2009) to investigate whether Stars 1 and 2 are similar to Milky Way field stars with similar colors, magnitudes, and velocities. We do the same for Stars 3 and 4, which we believe to be interlopers. We search for stars similar to Stars 1 and 2 by selecting SEGUE spectra of stars with the following restrictive set of properties: (1) $0.51 < (g - r)_0 < 0.55$, (2) $1.29 <$
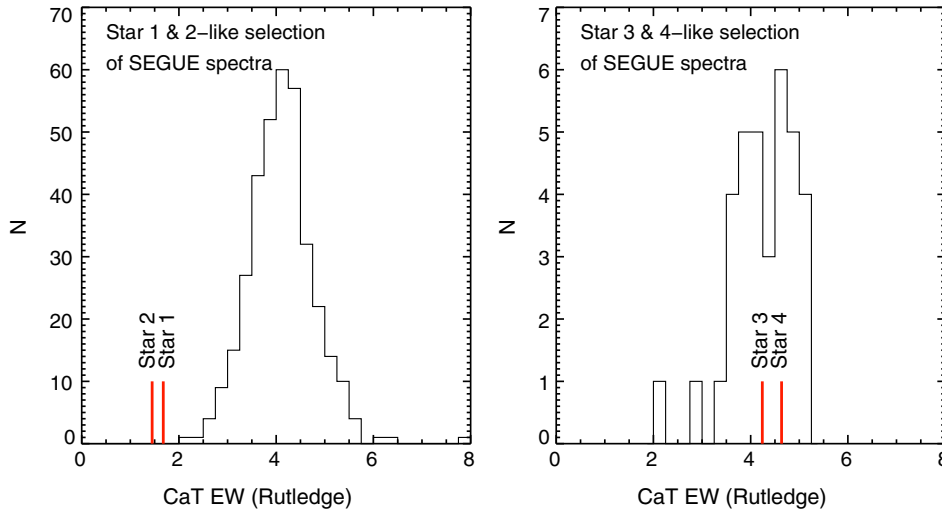
**Figure 6.** Histograms of the CaT EW measured from stellar spectra obtained from the SEGUE database. SEGUE stars were selected as those with color, apparent magnitude, and radial velocity extremely similar to those of Stars 1 and 2 or Stars 3 and 4 (criteria listed in Section 3.4). Stars 1 and 2 are both outliers from the 354 SEGUE stars with similar properties, showing that they are each inconsistent with being a foreground star. Even without the other evidence that Star 1 is a Wil 1 member star, this comparison implies the chance of Star 1 belonging to the Milky Way foreground to be less than 1/350. Conversely, Stars 3 and 4 are both very similar to the 35 SEGUE stars with similar properties, supporting our hypothesis that they are foreground stars.

(A color version of this figure is available in the online journal.)

$(u - g)_0 < 1.37$, (3) $18 < g_0 < 19$, and (4) a radial velocity between $-30$ and $0$. We search for stars similar to Stars 3 and 4 by selecting all SEGUE spectra of stars with the following: (1) $0.63 < (g - r)_0 < 0.67$, (2) $1.67 < (u - g)_0 < 1.74$, (3) $18 < g_0 < 19$, and (4) a radial velocity between $-30$ and $0$. We chose these photometric cuts based on the SDSS DR7 magnitudes of these stars (in Table 5). The reported SEGUE Stellar Parameter Pipeline quantities for the stars satisfying the Star 1/2-like (Star 3/4-like) criteria have a median [Fe/H] = $-0.65$ ($-0.7$) and log $g$ = 4.42 (4.47), indicating that the samples are dominated by thick disk dwarfs, as expected for the region of the CMD we are studying.

We downloaded the spectra of the 355 unique SEGUE stars satisfying Star 1/2-like criteria and of the 35 unique SEGUE stars satisfying the Star 3/4-like criteria. One spectrum of the 355 was excluded from analysis because it appeared to be flawed based on a visual inspection. We measured the CaT EW of each SEGUE spectrum in the same manner as for the Wil 1 stars, using the radial velocities given in the SEGUE database (median error = $2.5$ km s$^{-1}$). The distribution of CaT EW for the SEGUE stars is reasonably well-described as a Gaussian with a mean of 4.1 Å and a standard deviation of 0.6 Å. The histograms are shown in Figure 6.

No star in the Star 1/2-like SEGUE sample has a CaT EW < 2.2 Å. The Rutledge CaT EW of Star 1 is $1.68 \pm 0.3$ Å and Star 2 is $1.45 \pm 0.3$ Å—outliers from the SEGUE stars. The CaT EW of Star 1 is $2\sigma$ lower than the lowest of 354 stars in the SEGUE sample, showing that it is a true outlier from Milky Way foreground stars. Conversely, the stars in the Star 3/4-like SEGUE sample are very similar to Stars 3 and 4, which have CaT EW of $4.24 \pm 0.3$ Å and $4.64 \pm 0.3$ Å, respectively.

The spectral abundances of Stars 1 and 2 provide additional evidence against the hypothesis that either of them is a field Milky Way halo star. Using the spectral synthesis method of KGS08, described in Section 2.5, [Fe/H]$_{Star1}$ = $-1.73 \pm 0.12$, [Fe/H]$_{Star2}$ = $-2.65 \pm 0.12$, [Ca/Fe]$_{Star1}$ = $-0.4 \pm 0.18$, and [Ca/Fe]$_{Star2}$ = $+0.13 \pm 0.28$. Although its [Fe/H] is very similar

to the [Fe/H] of field halo stars, the [Ca/Fe] of Star 1 is much lower than that of typical halo stars (Venn et al. 2004). The [Fe/H] of Star 2 is also much lower than that of typical halo stars. In Section 4.1, we will discuss the abundances of Stars 1 and 2 in more detail.

Now that we have shown that neither Star 1 nor Star 2 is likely to be a foreground star, we compare their colors and absolute magnitudes with isochrones from the Dotter et al. (2008) library, and with the colors and absolute magnitudes of stars in the Draco dSph in Figures 7 and 8. We do this comparison to determine whether the very similar five-color SDSS photometry of Stars 1 and 2 (Table 5) can be consistent with the hypothesis that they are at the same distance but have very different metallicities. The Draco stars (black triangles) overplotted with Star 1 are those with $-2.0 <$ [Fe/H] $< -1.7$, as spectroscopically measured by Kirby et al. (2010). The Draco stars overplotted with Star 2 are those with $-3.4 <$ [Fe/H] $< -2.3$, as spectroscopically measured by Kirby et al. (2010).

These figures show that, for the most metal-poor stars, the models are largely consistent with the data in $g - r$ and $u - g$, but are too blue in $g - i$ and $u - z$. This discrepancy between models and data is qualitatively similar to that found by An et al. (2009), who showed that isochrones in the SDSS photometric system are systematically bluer than the colors of MS stars in relatively metal-poor GCs in $g - i$, $g - z$, and $u - g$.

These figures also show that stars belonging to Draco can have quite different spectroscopic metallicities, yet also have very similar colors in the SDSS filter set. Based on this comparison, we conclude that the similar five-color SDSS photometry of Stars 1 and 2 is consistent with our hypothesis that they both belong to Wil 1 and have [Fe/H] that differ by 1 dex.

Although our comparisons demonstrate that the simplest explanation for Stars 1 and 2 is that they belong to Wil 1 rather than the field halo, we cannot use this analysis to completely rule out the possibility that one is a halo star. For example, we could be unlucky and Wil 1 may lie in a direction and at a distance that has an excess of stellar halo structure with abundances atypical relative to other lines of sight. However, given all of
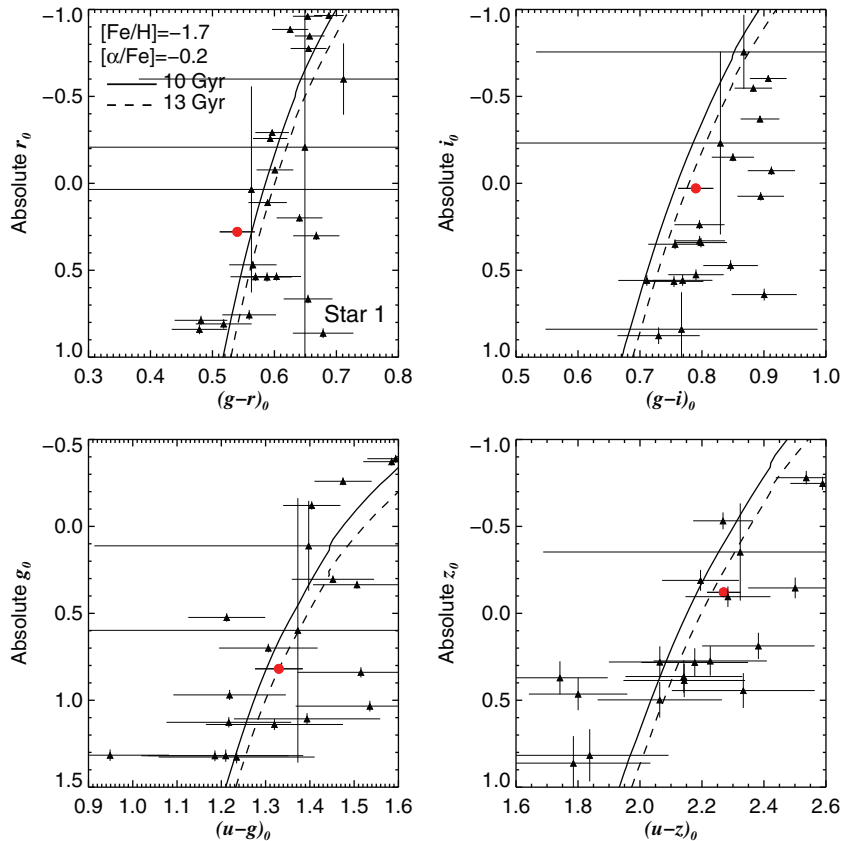
**Figure 7.** Color–magnitude diagrams showing Star 1 (red dot) compared to Draco stars (black triangles) and Dotter et al. (2008) isochrones. Draco stars with $-2.0 <$ [Fe/H] $< -1.7$, as measured by Kirby et al. (2010), are included in the figure. All magnitudes are de-reddened SDSS DR7 magnitudes, converted to absolute magnitudes. $1\sigma$ color–magnitude measurement uncertainties are shown for each star. The isochrone is [Fe/H] $= -1.7$, $[\alpha/\text{Fe}] = -0.2$ because it was the available isochrone that was closest to the measured $[\text{Fe/H}]_{\text{Star1}} = -1.73 \pm 0.12$, $[\text{Ca/Fe}]_{\text{Star1}} = -0.4 \pm 0.18$. We have offset the model $z$-isochrones by $-0.06$ mag and the model $i$-isochrones by $+0.03$ mag, to put them in the DR7 SDSS system (A. Dotter 2011, private communication).

(A color version of this figure is available in the online journal.)

the evidence, we conclude that Stars 1 and 2 are both Wil 1 members.

### 3.5. A Comparison with Other Methods of Identifying Interlopers

Other groups have used different approaches to identify likely Milky Way interlopers among spectroscopic samples of dwarf galaxy stars. The expectation maximization approach, tailored by Walker et al. (2009) for the study of Milky Way dwarf galaxies, combines the line-of-sight velocity, Mg EW, and projected position of each star in spectroscopic samples of Fornax, Carina, Sextans, and Sculptor stars to derive a probability that each star is a dwarf galaxy member rather than a contaminant star. While this approach is a powerful tool for studying the more luminous Milky Way galaxies, it is not easily applicable to the extremely low luminosity satellites. First, unlike the Walker et al. (2009) data sets, the spectroscopic samples of the extreme satellites tend to include stars with a wide range of surface gravities. Second, we want to drop the assumptions that the velocity distributions of stars in the extreme satellites are well described by Gaussians and that stars follow undisturbed exponential profiles out to large distances.

Another method frequently used to identify interlopers is the EW of the Na I line at 8190.5 Å. This line lies in our spectral range, is sensitive to both surface gravity and temperature, and has previously been used to discriminate between RGB stars and red MS stars. However, Gilbert et al. (2006) demonstrate

that while this spectral feature is very effective for dwarf/giant discrimination for $V - I > 2.5$, it is not effective for stars bluer than $V - I = 2.0$. The red giant members of Wil 1 in our sample have $0.4 < V - I < 1.0$, so we cannot use the Na I line to distinguish them from foreground dwarfs. It is possible that the use of this diagnostic by Martin et al. (2007) in their spectroscopic study of Wil 1 led to the inclusion of interlopers in their Wil 1 sample. For example, they classify our Star 4 as a member giant even though Siegel et al. (2008) show from a high-resolution spectrum that it is very likely to be a foreground dwarf.

### 3.6. Wil 1 Stars at Outlying Velocities?

To investigate the possibility that we missed one or more member stars associated with Wil 1 (bound or unbound), we looked at the five fRGB-colored stars at outlying velocities. The EWs of their Na I absorption lines are similar to those of likely Wil 1 members at similar apparent magnitudes. However, the surface gravities of fRGB stars associated with Wil 1 are not very different than those of Milky Way foreground stars in that region of the CMD. Even if this surface gravity indicator was robust for stars at these $g - r$ colors, it would not provide an effective discriminant. All five have higher CaT EWs than Wil 1 members at similar apparent magnitudes. We did not attempt this with MS/HB-colored stars because the error bars on all measured parameters are too large to provide a meaningful result. Although there could possibly be one, there is no obvious
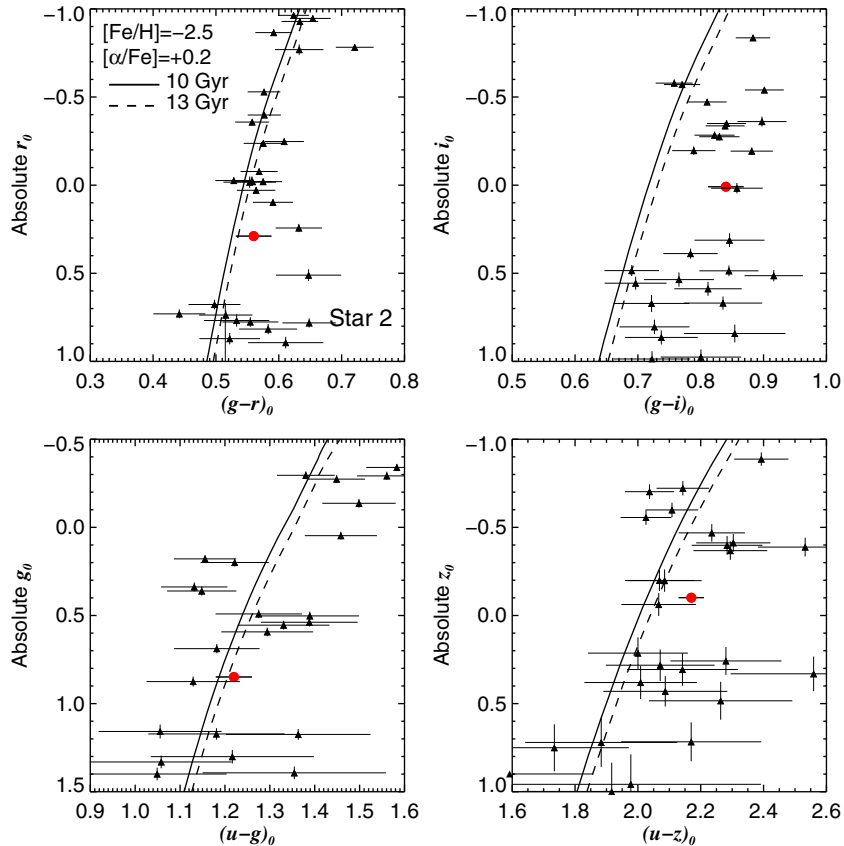
**Figure 8.** Same as Figure 7, but for Star 2 (red dot) plus Draco stars (black triangles) with [Fe/H] $< -2.3$ (includes stars with [Fe/H] as low as $-3.4$; Kirby et al. 2010). The isochrone is [Fe/H] $= -2.5$, [$\alpha$/Fe] $= +0.2$ because it was the available isochrone that was closest to the measured [Fe/H]$_{Star1} = -2.65 \pm 0.12$, [Ca/Fe]$_{Star2} = +0.13 \pm 0.28$.

(A color version of this figure is available in the online journal.)

candidate for a star associated with Wil 1 in the outlying tails of its velocity distribution.

## 4. THE NATURE OF WILLMAN 1: A DISRUPTING DWARF

### 4.1. An [Fe/H] Spread

Despite the observed star-to-star variations in some of the light elements, the Milky Way's GCs generally have not been observed to have a significant dispersion in [Fe/H] (e.g., Carretta et al. 2009). Although spectroscopic evidence exists for modest [Fe/H] spreads ($\sim$0.1–0.2 dex) in a small number of Milky Way GCs (e.g., M22 and M54; Da Costa et al. 2009; Carretta et al. 2010), only $\omega$Cen displays a large ($\sim$1 dex) star-to-star variation in [Fe/H] (e.g., Norris & Da Costa 1995). Owing to its unusual abundance distribution, $\omega$Cen is regarded to be the remaining core of an otherwise destroyed dwarf galaxy (Lee et al. 1999; Bekki & Freeman 2003). Unlike the GCs, all Milky Way dwarf galaxies are observed to have a significant dispersion in their stars' [Fe/H]. Observing such a spread is thus good evidence that an object self-enriched within a dark matter halo—that it is a galaxy.

Assessing the evidence for a metallicity spread in Wil 1 is challenging, because even minimal foreground contamination could lead to the erroneous conclusion that a large [Fe/H] spread exists. In Section 3.3, we applied a CaT $W'$ cut to reject possible foreground stars, leaving 10 highly probable member stars of the initial sample of 15 possible RGB members. This selection

left only Stars 1 and 2 of the five brightest possible member stars. We then performed a detailed analysis in Section 3.4 to ensure that Stars 1 and 2 are true Wil 1 members.

Using the spectral synthesis method of KGS08, described in Section 2.5, [Fe/H]$_{Star1} = -1.73 \pm 0.12$ and [Fe/H]$_{Star2} = -2.65 \pm 0.12$, indicating that Star 2 is 0.9 dex more iron-poor than Star 1. To show these results are not sensitive to S/N, we redo this analysis after artificially reducing the S/N in each spectrum by a factor of two with Gaussian random noise proportional to $\sqrt{\text{pixelvariance}}$. We find [Fe/H]$_{Star1} = -1.77 \pm 0.12$ and [Fe/H]$_{Star2} = -2.86 \pm 0.20$. The KGS08 technique also yields [Ca/Fe]$_{Star1} = -0.4 \pm 0.18$ and [Ca/Fe]$_{Star2} = +0.13 \pm 0.28$. This large spread of [Ca/Fe] abundances, with the more metal-rich star having the lower [Ca/Fe], is consistent with a scenario where Type Ia supernovae are controlling the chemical enrichment of Wil 1 after its first generation of stars. With only two bright RGB stars, it is unlikely that these spreads sample the full spread of abundances in Wil 1.

Stars 1 and 2 also have accurate photometry in SDSS DR7. We use the photometric metallicity calibration of Lenz et al. (1998): $l = -0.436u + 1.129g - 0.119r - 0.574i + 0.198$, valid in the range $0.5 < g - r < 0.8$. Stars with larger $l$ are more metal-poor. Stars 1 and 2 have $l = 0.137 \pm 0.032$ and $0.216 \pm 0.035$, respectively. Although there is no robust conversion between this Lenz photometric metallicity statistic and stellar metallicity, we use their calculations to estimate approximate photometric metallicities from the $l$ parameter. We fit a spline between $l$ and
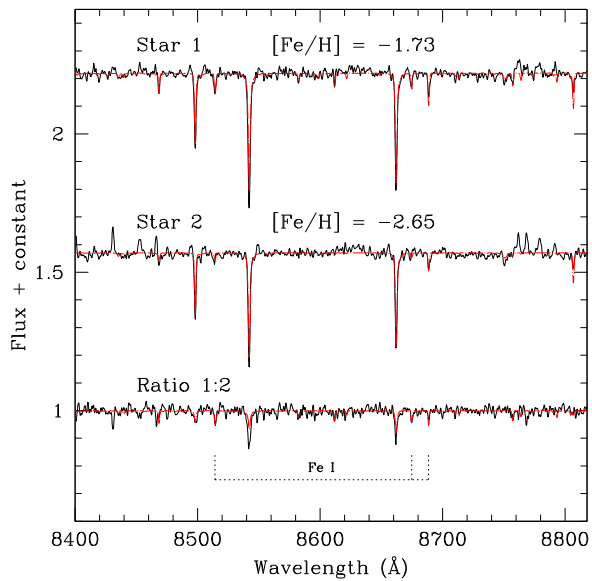
**Figure 9.** Portions of the spectra of Stars 1 and 2 (as listed in Table 2) around the Ca II triplet features. The bottom spectrum shows the ratio of these two stars; the clear features underscore the true difference in the abundances of these two Wil 1 member stars. The spectral syntheses used to measure [Fe/H] are overplotted.

(A color version of this figure is available in the online journal.)



**Figure 10.** Spatial distribution of the 40 Wil 1 member stars. For reference, dotted lines show 1, 2, 3, 4, 5, and 6 $R_{half}$ around the center of the object, oriented at a position angle of $77°$ (Martin et al. 2008a).
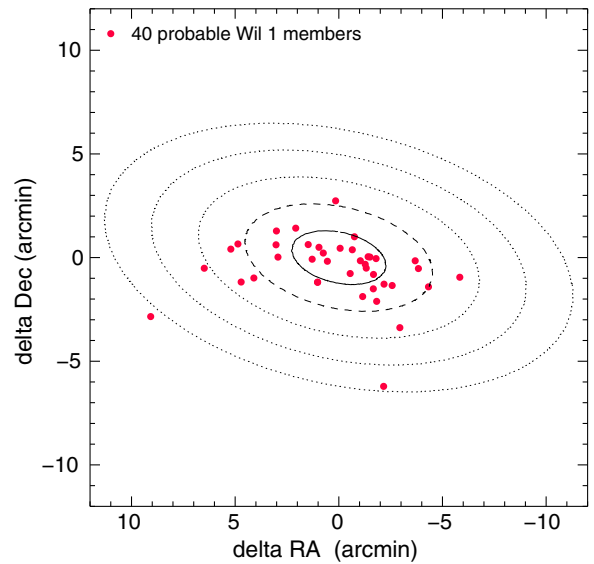
(A color version of this figure is available in the online journal.)

metallicity for the full set of their calculations shown in their Figure 8. This fit yields [M/H] estimates of $-1.8 \pm 0.3$ and $-3.0^{+0.7}_{-0.9}$ for Stars 1 and 2, respectively. Despite the significant random and (likely) systematic errors in this process, these values are consistent with our spectral synthesis measurements.

Figure 9 shows the spectra for these two stars in the region around the CaT along with the ratio of the spectra. The spectral syntheses used to measure [Fe/H] are overplotted. Visually, the individual spectra appear different, and weak lines can be seen in Star 1's spectrum that are not visible in Star 2's. The ratio of the spectra clearly shows that metal lines are stronger in Star 1. Given that the two stars have nearly identical luminosities and colors, this visual comparison also demonstrates that Star 1 is significantly more metal-rich than Star 2.

The scatter in $W'$ of the eight relatively faint Wil 1 RGB members seen in Figure 5 provides additional evidence for an internal abundance spread in this object. Taking the measurement uncertainties on $W'$ into account, these stars have a mean $W' = 2.4$ Å and a dispersion $= 0.7$ Å.

The method of KGS08 has been calibrated for stars with surface gravities lower than 3.6. Of the other eight probable Wil 1 RGB members, only one has log $g < 3.6$ (Star 8). We find that this star has [Fe/H] $= -1.92 \pm 0.21$. Averaging the [Fe/H] of Stars 1, 2, and 8, we find a mean [Fe/H] of $-2.1$. At face value, this is inconsistent with a simple linear metallicity–luminosity relation for Milky Way dwarf satellites. For example, the relation of Kirby et al. (2011) predicts a mean [Fe/H] $= -2.7$. Conversely, Kirby et al.'s (2011) linear relation predicts that the typical luminosity of a Milky Way satellite with [Fe/H] $= -2.1$ is $\sim 6.5 \times 10^4 L_{\odot}$. This offset between the observed and expected [Fe/H] of Wil 1 could result if the metallicity–luminosity relation flattens as the lowest luminosities (as also suggested by observations of Segue 1; Simon et al. 2011). Alternatively, it could result if Wil 1 has been stripped of a lot of its stellar mass, or if the mean [Fe/H]

based on three stars may not be an accurate reflection of the average composition of stars in this system.

For the purpose of comparison, the [Fe/H] derived for Stars 1 and 2 based on the Rutledge et al. (1997) calibration of CaT $W'$ are $-1.97 \pm 0.17$ and $-2.07 \pm 0.17$, respectively. The [Fe/H] derived for Stars 1 and 2 based on the Starkenburg et al. (2010) calibration of CaT $W'$ are $-2.36 \pm 0.20$ and $-2.64 \pm 0.29$, respectively. As expected, the Starkenburg et al. (2010) values are lower metallicity, because the Rutledge et al. (1997) [Fe/H] have been shown to systematically overestimate [Fe/H] lower than $-2.0$ (see KGS08; Starkenburg et al. 2010, and references therein). What is initially unexpected is that the [Fe/H] values of Stars 1 and 2 as derived using the CaT $W'$ as an [Fe/H] indicator underestimate the spread in [Fe/H] between Stars 1 and 2. This underestimate results from the large spread in [Ca/Fe] between Stars 1 and 2 and underscores another weakness of the CaT $W'$ approach to [Fe/H]. The CaT technique does not account for differences in [Ca/Fe]. If we compare the [Ca/H] we obtain using the relationship provided by Starkenburg et al. (2010) with the [Ca/H] derived through spectral synthesis, we find excellent agreement: $[Ca/H]_{Star1,Stark} = -2.11 \pm 0.20$ and $[Ca/H]_{Star1,Kirby} = -2.13 \pm 0.13$, $[Ca/H]_{Star2,Stark} = -2.39 \pm 0.29$ and $[Ca/H]_{Star2,Kirby} = -2.52 \pm 0.25$.

In summary, Wil 1 stars exhibit a substantial [Fe/H] spread. The [Fe/H] spread presented here is an underestimate if we have thrown out true member stars as a result of our $W'$ member selection criterion. We thus conclude that Wil 1 is a dwarf galaxy, or the remnants thereof.

### 4.2. Tentative Evidence for a Disturbed Morphology

The spatial distribution of Wil 1 stars displays tentative evidence for multi-directional features (Willman et al. 2006; Martin et al. 2007, although see Martin et al. 2008b and Walsh et al. 2008 for a discussion of shot noise and morphology) and has a moderately high ellipticity (Martin et al. 2008b; $e = 0.47 \pm 0.08$). Additionally, the spatial distribution of Wil 1's spectroscopic member stars provides tenuous evidence for an extended spatial distribution. Figure 10 shows that two of the

40 Wil 1 spectroscopic members lie at ∼5 $R_{half}$. Only 1% of the stars following an exponential distribution lie beyond 4 $R_{half}$. To test the likelihood of two outlying members occurring by chance in a system well described by an exponential distribution, we ran Monte Carlo simulations of the expected distribution of Wil 1 stars, assuming the (Martin et al. 2008b) structural parameters ($R_h = 2\overset{'}{.}3$; $\epsilon = 0.47$) and the target efficiency in Figure 5. In only 1.1% of simulations were there two or more stars between 4 and 6 $R_h$. Using the simulations described in Section 3.2, we find it unlikely that either of these stars is a contaminant. For example, there is a <2% chance that they are both foreground stars. These probabilities all depend on the assumption that Wil 1 is perfectly described by an exponential function (a larger fraction of a Plummer galaxy's light resides at large distance) and that its scale length is exactly that measured by Martin et al. (2008b). We thus consider these distant members to provide only tenuous evidence that Wil 1 may have an excess of stars at large radii, which could imply ongoing tidal stripping.

Each individual piece of evidence for a possible disturbed morphology of Wil 1 is not remarkable. When combined, they provide a reasonable (but still tentative) basis for believing that Wil 1 has been structurally disturbed, perhaps by the tidal field of the Milky Way.

## 5. THE KINEMATICS OF WIL 1

### 5.1. Dynamical Evidence for a High Dark Matter Content?

We begin by characterizing the global systemic velocity and velocity dispersion of Wil 1 with a single number, using the maximum likelihood method of Walker et al. (2006). This method assumes an intrinsic Gaussian distribution for the line-of-sight velocities of Wil 1 and adds in quadrature to the intrinsic dispersion the measurement error on each star. Though it is possible that the system could be bound, in dynamical equilibrium, and have a distribution function described by mild deviations from Gaussianity at all radii, the fact that the measurement errors are independent and Gaussian makes the Gaussian form of the likelihood an adequate general description of the system. Using the sample of 40 probable member stars, $v_{sys} = -14.1$ km s$^{-1}$ ± 1.0 km s$^{-1}$ and $\sigma_v = 4.0$ km s$^{-1}$ ± 0.8 km s$^{-1}$. If we also include the five more metal-rich stars flagged as probable contaminants in Section 3.3, $v_{sys} = -12.8$ km s$^{-1}$ ± 1.0 km s$^{-1}$ and $\sigma_v = 4.8$ km s$^{-1}$ ± 0.8 km s$^{-1}$. $3\sigma$ clipping removes no stars from either the 40 or the 45 star sample.

Given the line-of-sight velocity dispersion as calculated above, and assuming dynamical equilibrium, it is straightforward to estimate the mass of Wil 1. Wolf et al. (2010) use the sample of 40 probable member stars presented here and determine the mass within the half-light radius of $\sim 3.9^{+2.5}_{-1.6} \times 10^5 M_\odot$. This mass is relatively insensitive to the modeling of the velocity anisotropy profile and the parameterization of the light distribution of Wil 1. In terms of the central mass-to-light ratio, $(M/L)_V$, of $770^{+930}_{-440}$. A calculation including the five apparently metal-richer stars would imply a 40% larger mass. Even if all of the other assumptions were robust, we believe this higher inferred mass would be erroneous for the reasons given in Section 3.3.

### 5.2. An Unusual and Inconclusive Kinematic Distribution

We now investigate the kinematic distribution of Wil 1 stars in more detail. Is it even reasonable to characterize the systemic velocity and velocity dispersion of Wil 1 with a single number? Figure 11 shows the line-of-sight velocities of the probable
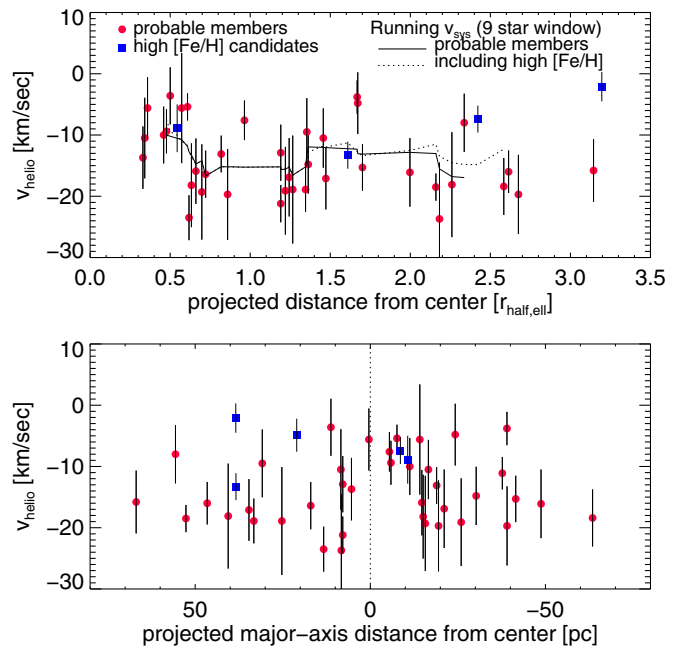


**Figure 11.** Heliocentric line-of-sight velocities of probable Wil 1 member stars high CaT $W'$ stars classified as possible interlopers in Section 3.3. Top panel: velocities as a function of two-dimensional elliptical distance from Wil 1's center, including the 38 probable members (of 40) and the 4 possible high [Fe/H] interlopers (of 5) with $r_{ell} < 3.5 r_{half}$. Overplotted is the systemic velocity of Wil 1, calculated in a nine star running window, calculated both with and without the possible interloper stars. Lower panel: the line-of-sight velocities of stars as a function of their one-dimensional projected distance along Wil 1's major axis, including the 39 probable members and the 5 possible high [Fe/H] interlopers with $d_{major} < 3.5$ 80 pc. The dotted line highlights the center of Wil 1. These panels show that neither is Wil 1's systemic velocity well described by a single value, nor is there clear evidence of rotation.

(A color version of this figure is available in the online journal.)

member stars (red circles) as a function of distance. The top panel shows elliptical distance from the center and the bottom panel shows distance along the major-axis relative to the center. Blue squares in both panels show the four stars within $3.5 r_{half}$ with CaT $W' > 3.9$ Å that we classified as likely interloper stars. Two member stars and one CaT $W' > 3.9$ Å star lie beyond the edge of both panels. We exclude these distant stars from further kinematic analysis because they may be remnants that have been stripped from the main body of the object (see Section 4.2).

Stars in the top panel of Figure 11 display an unusual kinematic distribution: central stars have velocities systematically offset from those of more distant member stars. The solid line shows the systemic velocity of Wil 1 calculated in a running window of nine stars, not including those identified with high [Fe/H]. The running $v_{sys}$ rapidly decreases by ∼8 km s$^{-1}$ from the center to the outskirts of Wil 1. The dotted line of Figure 11 shows the same as the solid line, but including the likely interloper stars. This line shows that our result is not affected by our criterion for interloper identification. It is tempting to invoke a tidally disrupting scenario may provide an explanation of this behavior in the systemic velocity, however this velocity distribution might not be easily explained by existing models of tidally stripped dwarf galaxies. For example, Klimentowski et al. (2009) show that different viewing angles of a stripped dwarf galaxy are expected to reveal a symmetric velocity distribution of unbound stream stars. We note that the details of this systemic velocity profile depend on the center used for Wil 1 and on the running window size. While we calculated Wil 1's

center (Section 2.1) as accurately as we could and the window size used here was not fine tuned to produce this result, if our center is inaccurate or if we choose a larger running window, we may not see such a striking shift in systemic velocity with distance. Given the relatively small kinematic sample from Wil 1 and its extreme faintness it is difficult to conclusively interpret this systemic velocity variation.

The bottom panel of Figure 11 shows that this unusual kinematic distribution is not obviously a result of ordered rotation. Visually, a model with velocity that is a linear function of major-axis position (as expected for ordered rotation) does not provide a good fit to these data. Additionally, even if the system were rotating with a reasonable velocity, this signal would not be able to be discerned with such a small sample of discrete velocities (Strigari 2010).

The variation in the systemic velocity with radius makes it difficult to robustly define the velocity dispersion of Wil 1. In fact we find the velocity dispersion profile of Wil 1 to be highly dependent on the running window or binsize used to calculate the profile. We therefore choose not to show a dispersion profile here. We note for the 40 Wil 1 members that (1) the velocity dispersion of the innermost eight stars is equal to $0 \, \text{km s}^{-1}$ with an uncertainty of $2.1 \, \text{km s}^{-1}$; (2) the velocity dispersion of the nine stars with distances between 1.0 and 1.5 $r_{\text{ell}}$ is also equal to $0 \, \text{km s}^{-1}$, with an uncertainty of $2.5 \, \text{km s}^{-1}$; and (3) the velocity dispersion of the outermost nine or ten stars shown in Figure 8 is equal to $0 \, \text{km s}^{-1}$, with an uncertainty of $2.1 \, \text{km s}^{-1}$. The details of this result are sensitive to the center used for Wil 1.

We now explicitly address each of the assumptions necessary for using the kinematics to interpret a high mass-to-light ratio for Wil 1. While these assumptions may be reasonable for many of the Milky Way's companions, it is not yet clear that they are reasonable assumptions for Wil 1.

1. *All 40 stars are physically associated with Wil 1.* As stated in Section 3, there may be a small number of Milky Way stars remaining in our sample of 40 likely Wil 1 members, likely among its apparent MS members. The velocity dispersions of the Milky Way halo and thick disk are larger than that measured for Wil 1, so stars belonging to them may somewhat artificially inflate the global velocity dispersion measured for Wil 1.

2. *All stars associated with Wil 1 are bound and in dynamical equilibrium.* Our sample of 40 contains too few stars to robustly check whether the velocity distribution of stars in Wil 1 is consistent with dynamical equilibrium. Its unusual spatial and velocity distributions (Figure 11 and discussed above), excess of spectroscopic members at large distance (Section 3.4), and its relatively high [Fe/H] for its luminosity (Section 5) may indicate that Wil 1 is a disrupted or disrupting object. If this were the case then the assumption of dynamical equilibrium would not be valid. It is plausible that the 40 member stars reported here may contain some (many) unbound stars.

3. *Contribution to velocities from binary stars.* Given the small velocity dispersion that we have measured, and the fact that the measurement uncertainties are similar to the measured velocity dispersion, it is possible that binary stars may be inflating the global line-of-sight velocity dispersion measured for Wil 1 stars. Minor et al. (2010) simulated the effect of binary stars observed velocity dispersions of dwarf spheroidal galaxies. They concluded that, while binaries do inflate the observed velocity dispersion of systems such as Wil 1, they are not expected to have inflated

the velocity dispersion of a system with $\sigma_{\text{obs}} = 4 \, \text{km s}^{-1}$ by more than $0.8 \, \text{km s}^{-1}$ over its $\sigma_{\text{intrinsic}}$. Alternative binary models have suggested that the observed dispersions of systems with intrinsic dispersions of only a few tenths of a $\text{km s}^{-1}$ could be even more affected by the presence of binaries (A. McConnachie 2010, private communication). Both modeling and repeated observations of individual Wil 1 member stars would be necessary to definitively conclude the effect of binaries on its observed velocity dispersion.

4. *Symmetric velocity distribution.* The distribution of line-of-sight velocities, relative to the mean velocity, is symmetric for any equilibrium galaxy model. While noting again that our sample size is too small to reach any statistically robust conclusion, there are initial hints of asymmetry in the line-of-sight velocity distribution (see Figure 8). If this asymmetric distribution persists with future data sets then it would support the hypothesis that Wil 1 is not a dynamically equilibrated system.

## 6. DISCUSSION AND CONCLUSIONS

The DEIMOS spectroscopic study presented here has revealed several new insights into the unusual Wil 1 object and has underscored the importance of careful foreground characterization when studying the least luminous Milky Way companions. We have shown that the velocity, color, and magnitude overlap of Wil 1's stellar population with foreground Milky Way stars make this object particularly difficult to study. We thus performed detailed Monte Carlo simulations to calculate the possible foreground contamination. We used CaT $W'$ plus color information to identify a total of five likely interloper stars out of the 45 possible spectroscopic members selected in Section 3.1. The high interloper fraction we estimated for Wil 1's brightest candidate RGB member stars does not imply that Wil 1's true luminosity is less than that derived in past studies. Photometric studies of ultra-faint dwarfs (e.g., Martin et al. 2007; Sand et al. 2009; Muñoz et al. 2010) typically use a statistical definition of their luminosity rather than adding up the light emitted from individual stars.

In concert with the Besancon Galaxy model, spectra from the SEGUE database helped confirmed the similarity of two of the five flagged interloper stars to Milky Way stars with similar color, magnitude, and velocity. SEGUE spectra also provided strong support for the presence of two true bRGB Wil 1 members (Stars 1 and 2 in Table 2, discussed in Section 3.4). SEGUE may thus provide a valuable resource for future studies that aim to eliminate interloper stars from spectroscopic samples.

The mean [Fe/H] of Wil 1's three confirmed RGB members with $\log g < 3.6$ is $-2.1$, with a difference of $0.9$ dex between the most metal-poor and metal-rich star. As discussed in Section 4.1, we interpret the large [Fe/H] difference between these stars to demonstrate that Wil 1 is (or once was) a dwarf galaxy, rather than a star cluster. With $r_0 \sim 18.1$ for the brighter two of these RGB members, they are good targets for high-resolution spectroscopic follow-up to investigate their detailed abundance patterns. Because Star 2 was observed by Siegel et al. (2008), Star 1 is the top priority for follow-up.

The kinematic distribution of Wil 1 is unlike the distribution yet seen in any of the Milky Way's satellites. Its inner nine spectroscopic member stars have radial velocities offset by $8 \, \text{km s}^{-1}$ from its 29 more distant members (excludes the two members more distant than 3.5 $r_{\text{half}}$). Neither published models of tidally disturbed satellites nor ordered rotation provide an

easy explanation for this distribution. We emphasize that the exact character of Wil 1's systemic velocity and velocity dispersion profile depends sensitively on the running window and the exact center used. We thus use this present data set to highlight the unusual nature of Wil 1's kinematics rather than to present definitive conclusions.

Wil 1's possible disturbed morphology and tentative excess of spectroscopic members at large distance relative to that of an undisturbed exponential distribution (Section 4.2) suggests that it may have been stripped of a substantial fraction of its stellar component. Some models of the tidal evolution of dark matter dominated satellites suggest that Wil 1 should presently have a high M/L even if it has suffered substantial tidal evolution (Peñarrubia et al. 2008). However, because its dark mass content cannot be well constrained given the reasons articulated above, appropriate caution must be taken when attempting to compare this object to the Milky Way's other satellites or attempting to use it to constrain the particle nature of dark matter.

If Wil 1 has been severely stripped of stars and the line-of-sight velocities of its stars do not trace the underlying gravitational potential, then why does it happen to lie on the $M_{\mathrm{dynamical}}/L_V$ versus $L_V$ relationship observed for Milky Way dwarf satellites (Geha et al. 2009; Wolf et al. 2010)? Perhaps this is a coincidence, or perhaps the velocities of Wil 1's stars do actually trace its gravitational potential, despite its overall unusual kinematic distribution. Only numerical models aimed specifically to reproduce Wil 1's properties may illuminate which answer is correct. Searches for dwarfs that can reveal the presence (or lack) of Wil 1-luminosity objects at a wide range of halo distances will be needed to know for certain the role of environment in shaping the luminosities of the tiniest Milky Way satellites.

## REFERENCES

Abazajian, K., & Sloan Digital Sky Survey, f. t. 2009, ApJS, 182, 543
Adelman-McCarthy, J. K., Agüeros, M. A., Allam, S. S., et al. 2006, ApJS, 162, 38
Aliu, E., Anderhub, H., Antonelli, L. A., et al. 2009, ApJ, 697, 1299
An, D., Pinsonneault, M. H., Masseron, T., et al. 2009, ApJ, 700, 523
Armandroff, T. E., & Da Costa, G. S. 1991, AJ, 101, 1329
Bekki, K., & Freeman, K. C. 2003, MNRAS, 346, L11
Belokurov, V., Walker, M. G., Evans, N. W., et al. 2008, ApJ, 686, L83
Belokurov, V., Zucker, D. B., Evans, N. W., et al. 2006, ApJ, 647, L111
Belokurov, V., Zucker, D. B., Evans, N. W., et al. 2007, ApJ, 654, 897
Belokurov, V., et al. 2009, MNRAS, 903
Blanton, M. R., & Roweis, S. 2007, AJ, 133, 734
Carretta, E., Bragaglia, A., Gratton, R., D'Orazi, V., & Lucatello, S. 2009, A&A, 508, 695
Carretta, E., Bragaglia, A., Gratton, R. G., et al. 2010, ApJ, 714, L7
Da Costa, G. S., Held, E. V., Saviane, I., & Gullieuszik, M. 2009, ApJ, 705, 1481
Dotter, A., Chaboyer, B., Jevremović, D., et al. 2008, ApJS, 178, 89
Essig, R., Sehgal, N., & Strigari, L. E. 2009, Phys. Rev. D, 80, 023506
Faber, S. M., Phillips, A. C., Kibrick, R. I., et al. 2003, Proc. SPIE, 4841, 1657
Geha, M., Willman, B., Simon, J. D., et al. 2009, ApJ, 692, 1464
Gilbert, K. M., Guhathakurta, P., Kalirai, J. S., et al. 2006, ApJ, 652, 1188
Harris, W. E. 1996, AJ, 112, 1487
Irwin, M. J., Belokurov, V., Evans, N. W., et al. 2007, ApJ, 656, L13
Jordi, K., Grebel, E. K., & Ammon, K. 2006, A&A, 460, 339
Kirby, E. N., Guhathakurta, P., Simon, J. D., et al. 2010, ApJS, 191, 352
Kirby, E. N., Guhathakurta, P., & Sneden, C. 2008a, ApJ, 682, 1217
Kirby, E. N., Lanfranchi, G. A., Simon, J. D., Cohen, J. G., & Guhathakurta, P. 2011, ApJ, 727, 78
Kirby, E. N., Simon, J. D., Geha, M., Guhathakurta, P., & Frebel, A. 2008b, ApJ, 685, L43
Klimentowski, J., Łokas, E. L., Kazantzidis, S., et al. 2009, MNRAS, 400, 2162
Koch, A., Wilkinson, M. I., Kleyna, J. T., et al. 2009, ApJ, 690, 453
Koposov, S., de Jong, J. T. A., Belokurov, V., et al. 2007, ApJ, 669, 337
Law, D. R., & Majewski, S. R. 2010, ApJ, 718, 1128
Lee, Y., Joo, J., Sohn, Y., et al. 1999, Nature, 402, 55
Lenz, D. D., Newberg, J., Rosner, R., Richards, G. T., & Stoughton, C. 1998, ApJS, 119, 121
Loewenstein, M., & Kusenko, A. 2010, ApJ, 714, 652
Martin, N. F., Coleman, M. G., De Jong, J. T. A., et al. 2008a, ApJ, 672, L13
Martin, N. F., de Jong, J. T. A., & Rix, H.-W. 2008b, ApJ, 684, 1075
Martin, N. F., Ibata, R. A., Chapman, S. C., Irwin, M., & Lewis, G. F. 2007, MNRAS, 380, 281
Minor, Q. E., Martinez, G., Bullock, J., Kaplinghat, M., & Trainor, R. 2010, ApJ, 721, 1142
Muñoz, R. R., Carlin, J. L., Frinchaboy, P. M., et al. 2006, ApJ, 650, L51
Muñoz, R. R., Geha, M., & Willman, B. 2010, AJ, 140, 138
Niederste-Ostholt, M., Belokurov, V., Evans, N. W., et al. 2009, MNRAS, 398, 1771
Norris, J. E., & Da Costa, G. S. 1995, ApJ, 447, 680
Peñarrubia, J., Navarro, J. F., & McConnachie, A. W. 2008, ApJ, 673, 226
Robin, A. C., Reylé, C., Derrière, S., & Picaud, S. 2003, A&A, 409, 523
Rutledge, G. A., Hesser, J. E., & Stetson, P. B. 1997, PASP, 109, 907
Ryan, S. G., & Norris, J. E. 1991, AJ, 101, 1865
Sakamoto, T., & Hasegawa, T. 2006, ApJ, 653, L29
Sand, D. J., Olszewski, E. W., Willman, B., et al. 2009, ApJ, 704, 898
Schlegel, D. J., Finkbeiner, D. P., & Davis, M. 1998, ApJ, 500, 525
Siegel, M. H., Shetrone, M. D., & Irwin, M. 2008, AJ, 135, 2084
Simon, J. D., & Geha, M. 2007, ApJ, 670, 313
Simon, J. D., Geha, M., Minor, Q. E., et al. 2011, ApJ, 733, 46
Sohn, S. T., Majewski, S. R., Muñoz, R. R., et al. 2007, ApJ, 663, 960
Starkenburg, E., Hill, V., Tolstoy, E., et al. 2010, A&A, 513, A34
Strigari, L. E. 2010, Adv. Astron., 407394
Strigari, L. E., Bullock, J. S., Kaplinghat, M., et al. 2008a, Nature, 454, 1096
Strigari, L. E., Koushiappas, S. M., Bullock, J. S., et al. 2008b, ApJ, 678, 614
Tollerud, E. J., Bullock, J. S., Strigari, L. E., & Willman, B. 2008, ApJ, 688, 277
Venn, K. A., Irwin, M., Shetrone, M. D., et al. 2004, AJ, 128, 1177
Walker, M. G., Mateo, M., Olszewski, E. W., Sen, B., & Woodroofe, M. 2009, AJ, 137, 3109
Walker, M. G., Mateo, M., Olszewski, E. W., et al. 2006, AJ, 131, 2114
Walsh, S. M., Jerjen, H., & Willman, B. 2007, ApJ, 662, L83
Walsh, S. M., Willman, B., & Jerjen, H. 2009, AJ, 137, 450
Walsh, S. M., Willman, B., Sand, D., et al. 2008, ApJ, 688, 245
Willman, B., Blanton, M. R., West, A. A., et al. 2005a, AJ, 129, 2692
Willman, B., Dalcanton, J. J., Martinez-Delgado, D., et al. 2005b, ApJ, 626, L85
Willman, B., Masjedi, M., Hogg, D. W., et al. 2006, arXiv:astro-ph/0603486
Wolf, J., Martinez, G. D., Bullock, J. S., et al. 2010, MNRAS, 406, 1220
Yanny, B., Rockosi, C., Newberg, H. J., et al. 2009, AJ, 137, 4377
Zucker, D. B., Belokurov, V., Evans, N. W., et al. 2006a, ApJ, 650, L41
Zucker, D. B., Belokurov, V., Evans, N. W., et al. 2006b, ApJ, 643, L103